



# Study of disorders in regulatory spatiotemporal neurodynamics of calcium and nitric oxide

Anand Pawar<sup>1</sup> · Kamal Raj Pardasani<sup>1</sup>

Received: 1 June 2022 / Revised: 26 September 2022 / Accepted: 14 October 2022 / Published online: 8 November 2022  
© The Author(s), under exclusive licence to Springer Nature B.V. 2022

## Abstract

Experimental studies have reported the dependence of nitric oxide (NO) on the regulation of neuronal calcium ( $[Ca^{2+}]$ ) dynamics in neurons. But, there is no model available to estimate the disorders caused by various parameters in their regulatory dynamics leading to various neuronal disorders. A mathematical model to analyze the impacts due to alterations in various parameters like buffer, ryanodine receptor, serca pump, source influx, etc. leading to regulation and dysregulation of the spatiotemporal calcium and NO dynamics in neuron cells is constructed using a system of reaction–diffusion equations. The numerical simulation is performed with the finite element approach. The disturbances in the different constitutive processes of  $[Ca^{2+}]$  and nitric oxide including source influx, buffer mechanism, ryanodine receptor, serca pump,  $IP_3$  receptor, etc. can be responsible for the dysregulation in the  $[Ca^{2+}]$  and NO dynamics in neurons. Also, the results reveal novel information about the magnitude and intensity of disorders in response to a range of alterations in various parameters of this neuronal dynamics, which can cause dysregulation leading to neuronal diseases like Parkinson's, cerebral ischemia, trauma, etc.

**Keywords** Reaction–diffusion equations · Calcium dynamics · Nitric oxide · Neuron cell · Finite element approach

## Introduction

Nitric oxide being signaling molecule affects numerous biological activities in neuromuscular (Stamler and Meissner 2001), immunological (Bogdan 2001), and other pathways (Davis et al. 2001). NO signaling is essential in neurotransmitter release, learning, memory, and neuronal excitability (Kiss et al. 2001; Prast et al. 2001; Boehning et al. 2003). Nitric oxide has toxic as well as beneficial effects on different cells in the human body. Tsoukias (2008) investigated the various processes, which affect the availability of nitric oxide in health and diseases. Experimental studies suggested that nitroglycerine, nitrates, and guanylate cyclase are helpful to relax the smooth muscles

of the heart due to the significant NO impacts. Garthwaite (1991) explored the importance of NO signaling in nerve cells. The overproduction and accumulation of NO may result in neuronal injury and cell death via neurotoxicity, proteins modifications, and damage of DNA (Zhang et al. 2006). The nitric oxide-induced neurotoxicity leads to neuronal disorders (Torreilles et al. 1999) including Parkinson's (Zhang et al. 2006), primary headache (Thomsen 2001), HIV-related dementia (Kaul et al. 2001), stroke (Lo et al. 2003), etc. The neurotoxicity is mediated by NMDAR due to the involvement of nitric oxide leads to neuronal cell death underlying numerous neuronal diseases (Dawson et al. 1991). Also, the protein modifications by nitric oxide via the involvement of reactive cysteine thiols (S-nitrosylation) lead to neuronal cell death (Lipton et al. 1993). Nitric oxide has cytoprotective properties in nerve cells at low concentrations, but it becomes detrimental at high concentrations by inducing cytotoxic effects on the cells (Kourosh-Arami et al. 2020).

The mathematics of diffusion and its significance in various media such as plane sheets, cylinders, etc. have been discussed by Crank (1979). The regulation of genome

---

✉ Anand Pawar  
ap.193104003@manit.ac.in  
Kamal Raj Pardasani  
kamalraj@rediffmail.com

<sup>1</sup> Department of Mathematics, Bioinformatics and Computer Applications, Maulana Azad National Institute of Technology, Bhopal, Madhya Pradesh 462003, India

expression, hormone release, dendroplasmic flow, etc. by calcium mechanism in neuron cells has been examined by Llinas (1979). The presynaptic calcium transport model in the presence of buffer, pump, and various channels in nerve cells has been explored by Fogelson and Zucker (1985). The influence of buffer capacity on the regulatory  $[Ca^{2+}]$  processes in neuron cells has been discussed by Ahmed and Connor (1988). In neurons, the elementary calcium processes such as calcium release and calcium entry are associated with different channels (Bootman and Berridge 1995). The mathematical models of calcium diffusion with buffer approximation and validation in the nerve cell were constructed by Wagner et al. (1994) and Smith et al. (1996), Smith (1996). The rapid transit of  $[Ca^{2+}]$  ions via the channels in neurons causes the oscillatory behavior of calcium (Egelman and Montague 1999). The high concentration of slow buffer also creates oscillations in the neuronal calcium signaling (Falcke 2003). The endoplasmic reticulum (ER) regulates the diverse signaling events in a neuron cell (Verkhatsky 2002). The calcium diffusion model and significance of different channels such as ryanodine receptor and  $IP_3$  in acinar cells have been examined by Sneyd et al. (2003). The neuronal pathologies are associated with the dysfunction of calcium signaling in neurons (Brini et al. 2014). In the last decade, numerous authors have explored calcium regulation in different cells including astrocytes (Jha et al. 2013, 2014), neurons (Tewari et al. 2008, 2010, 2011, 2012; Tripathi et al. 2011; Jha et al. 2014), acinar (Manhas and Pardasani 2014, Manhas et al. 2014), myocyte (Pathak et al. 2015, 2016), Oocyte (Panday et al. 2013; Naik and Pardasani 2015b, 2016, 2019), etc. using different analytical and numerical procedures. The calcium transport model with the presence of excess buffer and sodium ions in neurons has been explored by Tewari et al. (2011). The consequences of excess buffer and VGCC on calcium dynamics in astrocyte cell has been discussed by Jha et al. (2013, 2014). The influences of different processes such as buffer, pump, and leak on calcium dynamics in the myocytes and fibroblast cells have been studied by Pathak et al. (2015, 2016) and Kotwani et al. (2012, 2014), respectively. The finite element model has been constructed by Naik and Pardasani (2013) to study the effects of numerous different parameters such as  $Na^+/K^+$  pump, buffer,  $Na^+/Ca^{2+}$  exchanger, etc. on  $[Ca^{2+}]$  signaling in Oocytes. Also, Naik and Pardasani (2015b) explored the calcium signaling for two-dimensional cases using a finite element procedure to examine the influences of various parameters including ryanodine receptor, serca pump, etc. in Oocytes cells. Naik and Pardasani (2019) examined that various mechanisms such as diffusion, buffer, VGCC, serca pump, RyR, etc. regulate the calcium concentration level in Oocytes. The spatiotemporal calcium model incorporating ER leak,

VGCC, buffer, and extrusion of calcium mechanism in T lymphocytes has been discussed by Naik and Zu (2020) to explore the applications of the model in cell protection and strengthening immune systems. Eskandari et al. (2021) discussed the time-discrete chemical model for two-dimensional cases and fixed points existence to detect the flip and generalized flip bifurcations. Jagtap and Adlakha (2018) explored the importance of the buffer mechanism in calcium distribution in hepatocyte cells. The calcium release from ER through the  $IP_3$ -sensitive channel in neuron cells has been discussed by Falcke et al. (2000) to explore the functions of calcium and  $IP_3$  in chaotic oscillations. The  $IP_3$  production depends on the calcium-sensitive pathway, which is activated by calcium waves. The positive feedback of calcium and  $IP_3$ -induced calcium release enhances the  $IP_3$  production by simulating PLC in the cell (Miyazaki 1993). The  $IP_3$  production, which is caused by calcium activation either by PLC or by a subunit of G protein, and the physiological ranges of  $IP_3$  production (0.1–3.0  $\mu M$ ) have been explored by Young and Keizer (1992). In the case of calcium oscillations, the calcium feedback on the  $IP_3$  degradation pathways has been discussed by Dupont and Erneux (1997).

The association of nitric oxide with numerous secondary signaling molecules including  $[Ca^{2+}]$ , proteins, and oxygen has a significant impact on cellular regulation processes. The calcium concentration increases initially due to the intracellular  $[Ca^{2+}]$  release and the elevated calcium can cause NO generation in the cells. The nitric oxide production is simulated by calcium influx, which is induced by a glutamate receptor in a neuron cell (Garthwaite et al. 1989; Wood et al. 1990). The calcium-dependent and calcium-independent nitric oxide formation and biological significance of NO in different tissues have been explored by Salter and Knowles (1991). The deficiency of calcium can cause deficient nitric oxide production, which leads to preeclampsia disease in women (López-Jaramillo 2000). In the tissues, the calcium-dependent production of nitric oxide is induced by sex hormones (Weiner et al. 1994). In the past, various researchers studied the NO production and regulation in nerve cells (Bredt et al. 1990; Aimi et al. 1993; Ceccatelli et al. 1994; Vincent 1994). Vincent (2010) explored the functions of VGCC in nitric oxide production in neurons. Also, R-type calcium channels are essential in nitric oxide generation in the nerve cell (Kohlmeier and Leonard 2006). The nitric oxide signaling requires tight regulation by calcium to prevent the cell from neurotoxicity (Brenman et al. 1997). The impact of NO on  $[Ca^{2+}]$  ion channels in vascular smooth muscle, such as calcium-dependent potassium channels has been examined by Bolotina et al. (1994). The nitric oxide signaling acts as an amplifier of calcium signals in a neuron cell (Peunova and Enikolopov 1993). Furthermore, NO may have a protective

impact by neutralizing superoxide ions and preventing oxygen radical damage to cerebellar cells (Garthwaite et al. 1988). The nitric oxide concentration is reported to be in the range 0 to 500 nmol ( $10^{-3}$   $\mu$ M) (Wood and Garthwaite 1994) in the neuron cells. Dormanns et al. (2016) and Plank et al. (2007) developed mathematical models to study the calcium signaling and nitric oxide generation in the neurons. The voltage-dependent calcium channels elevate the cytosolic calcium concentration that produces nitric oxide by binding neuronal NO synthase (Kourosh-Arabi et al. 2020). The IP<sub>3</sub> receptor needs calcium concentration for channel activation even in the existence of IP<sub>3</sub> and it enhances calcium levels in cells. The generation of effective vasodilators like nitric oxide in the cell regulates the high calcium concentration (Iino 2006). Thus, the process of NO production controls the elevated calcium in nerve cells. The serca pump activities are increased by the nitric oxide (NO) through the reactive cysteine-674 in the endoplasmic reticulum (ER), which can further lead to the inhibition of calcium influx in the cell (Tong et al. 2008). The alterations in serca pump mechanism can cause the different neuronal disorders including Alzheimer's. The effects of nitric oxide on serca pump activities are crucial to understand as the dysregulation in serca pump mechanism can be responsible for the dysregulation in other ER mechanisms. The dysregulation in [Ca<sup>2+</sup>] and NO levels in cells can be responsible for different neuronal disorders such as Ischemia, Alzheimer's, etc. The elevation in neuronal calcium concentration is associated with Ischemia (Chung et al. 2015). Bodalia et al. (2013) experimentally investigated that during Ischemia, the IP<sub>3</sub> and ryanodine receptors cause the aberrant [Ca<sup>2+</sup>] release from ER, and the impaired reuptake of cytosolic calcium to ER via serca pump elevates the calcium levels. Also, the elevated calcium concentration during Ischemia can produce a high amount of NO (Moro et al. 2004). Wojda et al. (2008) reported that the alteration in the [Ca<sup>2+</sup>] homeostasis including impaired calcium reuptake through serca pump, disturbances in source influx, etc. are associated with Ischemia, which further leads to rapid cell death.

Manhas et al. (2014) examined the fluctuations in the calcium signaling due to the IP<sub>3</sub> mechanism in the acinar cell. In recent years, the cooperation of [Ca<sup>2+</sup>] and IP<sub>3</sub> in the myocyte and hepatocyte cells have been explored by Singh et al. (2019a, 2019b, 2020) and Jagtap et al. (2019), respectively. Pawar and Pardasani (2022a) examined the dysregulatory effects of [Ca<sup>2+</sup>] and IP<sub>3</sub> signaling on the NO and  $\beta$ -amyloid formation in nerve cells. Also, the cooperative regulation and dysregulation of [Ca<sup>2+</sup>] and  $\beta$ -amyloid have been explored by Pawar and Pardasani (2022a) to study the effect of disturbances in different processes on the calcium and  $\beta$ -amyloid in neuron cells. Very few researchers studied the temporal

dependence of NO on [Ca<sup>2+</sup>] dynamics in nerve cells. However, no research on the spatiotemporal dependence of nitric oxide dynamics on [Ca<sup>2+</sup>] dynamics in nerve cells has been reported. Also, the earlier models have not taken into consideration the association of neuronal disorders due to the disturbances in the constitutional processes of the different parameters of spatiotemporal dynamics of calcium and NO in neuron cells. The exploration of the spatiotemporal dependence of NO on calcium regulation can be crucial for providing therapeutic and curative interventions for neuronal disorders.

The present focus is on exploring the regulatory and dysregulatory impacts of the spatiotemporal dynamics of [Ca<sup>2+</sup>] and NO in nerve cells. The findings were achieved using a finite element procedure and the influences of diverse parameters on the [Ca<sup>2+</sup>] and NO dynamics have been examined in neurons.

## Mathematical formulation

Involving the buffer (EGTA) and ryanodine receptor in Wagner et al. (2004) model, and the [Ca<sup>2+</sup>] regulation with constant IP<sub>3</sub> can be expressed in the neurons as,

$$\frac{\partial [\text{Ca}^{2+}]}{\partial t} = D_{\text{Ca}} \frac{\partial^2 [\text{Ca}^{2+}]}{\partial x^2} + \left( \frac{J_{\text{IPR}} - J_{\text{SERCA}} + J_{\text{LEAK}} + J_{\text{RyR}}}{F_{\text{C}}} \right) - K^+ [\text{B}]_{\infty} \left( [\text{Ca}^{2+}] - [\text{Ca}^{2+}]_{\infty} \right), \quad (1)$$

where,  $D_{\text{Ca}}$  represents the [Ca<sup>2+</sup>] diffusion coefficient.  $[\text{B}]_{\infty}$  and  $[\text{Ca}^{2+}]_{\infty}$  are respectively the steady-state buffer and [Ca<sup>2+</sup>] concentrations.  $K^+$  denotes the buffer association rate and 'x', and 't' represent the position and time variables.

Wagner et al. (2004) provides the numerous influxes and outfluxes of Eq. (1), as shown below,

$$J_{\text{IPR}} = V_{\text{IPR}} m^3 h^3 \left( [\text{Ca}^{2+}]_{\text{ER}} - [\text{Ca}^{2+}] \right), \quad (2)$$

$$J_{\text{SERCA}} = V_{\text{SERCA}} \left( \frac{[\text{Ca}^{2+}]^2}{[\text{Ca}^{2+}]^2 + K_{\text{SERCA}}^2} \right), \quad (3)$$

$$J_{\text{LEAK}} = V_{\text{LEAK}} \left( [\text{Ca}^{2+}]_{\text{ER}} - [\text{Ca}^{2+}] \right), \quad (4)$$

$$J_{\text{RyR}} = P_0 V_{\text{RyR}} \left( [\text{Ca}^{2+}]_{\text{ER}} - [\text{Ca}^{2+}] \right), \quad (5)$$

where,  $J_{\text{IPR}}$ ,  $J_{\text{LEAK}}$ , and  $J_{\text{RyR}}$  are the fluxes due to IP<sub>3</sub>-receptor, ER, and ryanodine receptor respectively. The serca pump efflux is denoted by  $J_{\text{SERCA}}$ .  $V_{\text{LEAK}}$ ,  $V_{\text{IPR}}$ ,  $V_{\text{SERCA}}$ , and  $V_{\text{RyR}}$  are respectively denoting the flux rate constants for leak, IP<sub>3</sub> receptor, pump (serca), and ryanodine receptor.  $K_{\text{SERCA}}$  denotes the Michaelis constant for

serca pump.  $P_0$  denotes the probability for ryanodine receptor.

Li and Rinzel (1994) provides the expressions for  $m$  and  $h$ , which are displayed below.

$$m = \left( \frac{[IP_3]}{[IP_3] + K_{IP_3}} \right) \left( \frac{[Ca^{2+}]}{[Ca^{2+}] + K_{Ac}} \right), \tag{6}$$

$$h = \frac{K_{Inh}}{K_{Inh} + [Ca^{2+}]}, \tag{7}$$

where variable  $h$  indicates the fraction of subunit not yet activated via calcium. The constants of the binding positions of activating  $IP_3$ , activating  $[Ca^{2+}]$  and inhibiting  $[Ca^{2+}]$  are respectively indicated by  $K_{IP_3}$ ,  $K_{Ac}$ , and  $K_{inh}$ .

The nitric oxide dynamics incorporating calcium provided by Gibson et al. (2007) is shown below,

$$\frac{\partial [NO]}{\partial t} = D_{NO} \frac{\partial^2 [NO]}{\partial x^2} + (J_{production} - J_{degradation}), \tag{8}$$

where  $D_{NO}$  denotes the nitric oxide diffusion coefficient. The nitric oxide production flux is described by Gibson et al. (2007) as,

$$J_{production} = V_{NO} \left( \frac{[Ca^{2+}]}{[Ca^{2+}] + K_{NO}} \right), \tag{9}$$

where  $J_{Production}$  represents the nitric oxide production flux.  $V_{NO}$  and  $K_{NO}$  are the rate constants.

$$J_{degradation} = K_{deg}[NO], \tag{10}$$

where the flux term for nitric oxide degradation is represented by  $J_{degradation}$  and  $K_{deg}$  represents the degradation rate constant for nitric oxide in the cell.

The  $[Ca^{2+}]_{ER}$  may be estimated by the total concentration of cellular  $[Ca^{2+}]$  conservation relationship,

$$[Ca^{2+}]_T = F_E [Ca^{2+}]_{ER} + F_C [Ca^{2+}]_C, \tag{11}$$

where  $[Ca^{2+}]_{ER}$  is the  $[Ca^{2+}]$  levels in ER. The volume fraction corresponding to the total cell volume of cytosol and ER are sequentially represented by  $FC$  and  $FE$ .

### Initial conditions

For  $[Ca^{2+}]$  and  $NO$ , the initial concentrations are given respectively by Dupont et al. (2000) and Van Liew and Raychaudhuri (1997), as follows,

$$[Ca^{2+}]_{t=0} = 0.1 \mu M, \tag{12}$$

$$[NO]_{t=0} = 0 \mu M, \tag{13}$$

### Boundary conditions

Brown et al. (2008) provides the boundary condition for  $[Ca^{2+}]$  as shown below,

$$\lim_{x \rightarrow 0} \left( -D_c \frac{\partial [Ca^{2+}]}{\partial x} \right) = \sigma, \tag{14}$$

where, source influx is denoted by  $\sigma$ .

$[Ca^{2+}]$  level reaches  $0.1 \mu M$  with distant near the source,

$$\lim_{x \rightarrow 5} [Ca^{2+}] = [Ca^{2+}]_{\infty} = 0.1 \mu M, \tag{15}$$

The boundary conditions of  $NO$  dynamics are given by Kavdia et al. (2002) as expressed below,

$$\lim_{x \rightarrow 0} \left( \frac{\partial [NO]}{\partial x} \right) = 0. \tag{16}$$

$$\lim_{x \rightarrow 5} \left( \frac{\partial [NO]}{\partial x} \right) = 0. \tag{17}$$

In the Appendix, the description of the finite element approach utilized to solve the systems equations with the initial and boundary concentrations has been presented.

### Results and discussion

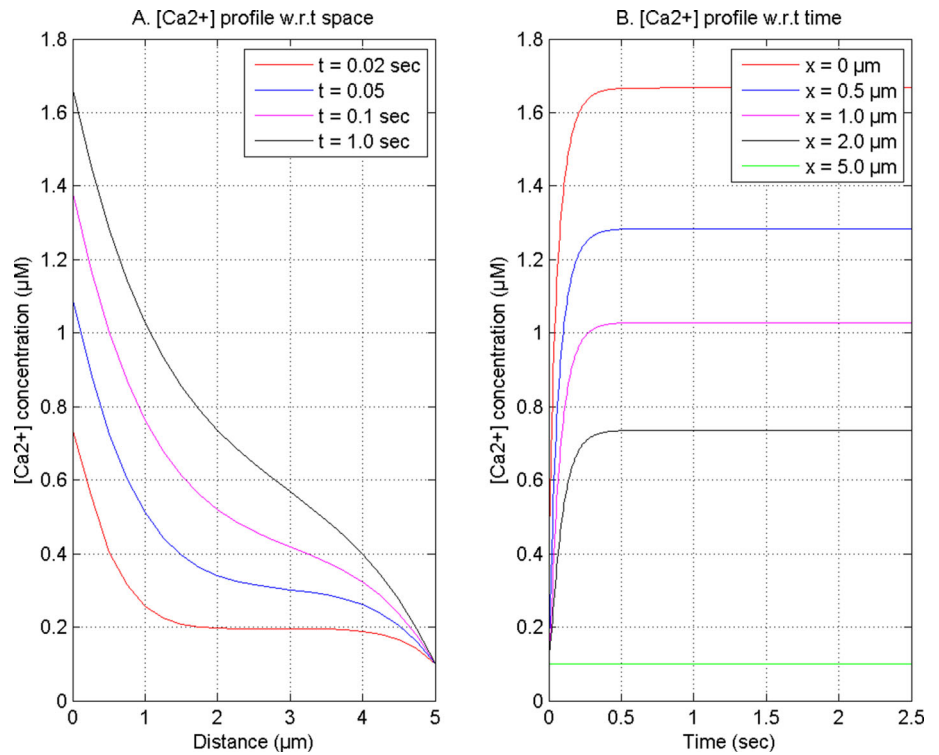
Graphs are used to display the numerical findings of the system of equations. Table 1 exhibits the numerical values of the several variables utilized in this study.

Figure 1 exhibits the spatiotemporal calcium distribution at various time and position instants in nerve cells. The influences of the calcium diffusion, buffer mechanism, and calcium handling by the ER on  $IP_3$ -mediated calcium release through  $IP_3$ -receptor, calcium-mediated calcium release through ryanodine receptor, and the reuptake of calcium from cytosol to ER by serca pump on calcium signaling have been noticed in Fig. 1. The spatial  $[Ca^{2+}]$

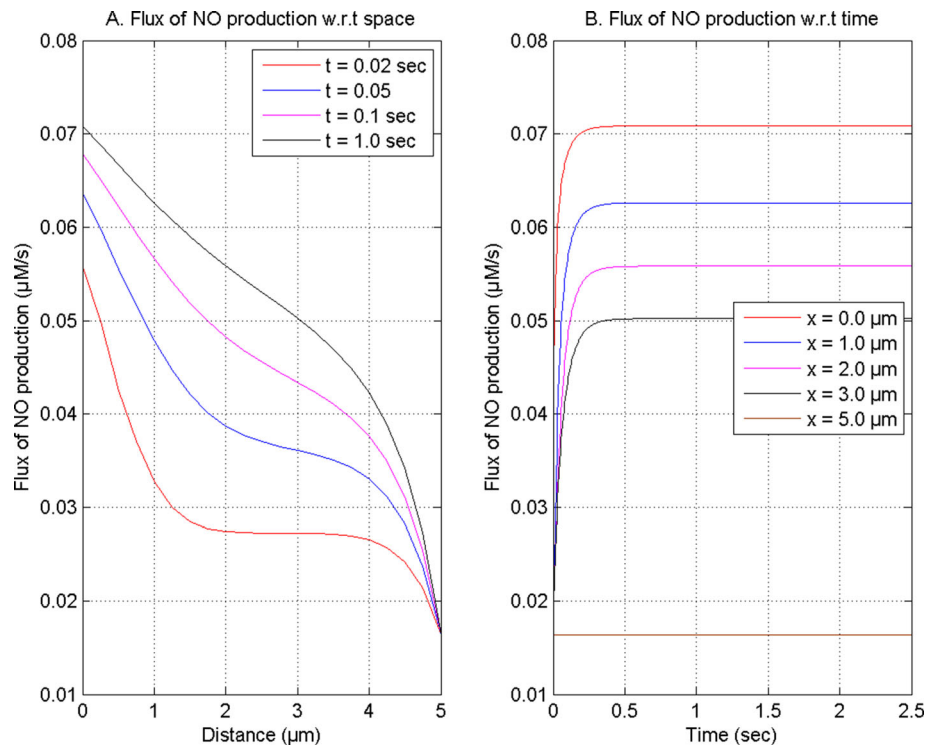
**Table 1** Parameters with numerical data [Wagner et al. (2004) and Gibson et al. (2007)]

Symbols	Values	Symbols	Values
$V_{IPR}$	$8.5 s^{-1}$	$K_{IP3}$	$0.15 \mu M$
$K_{serca}$	$0.4 \mu M$	$V_{serca}$	$0.65 \mu M/s$
$V_{Leak}$	$0.01 s^{-1}$	$K_{Ac}$	$0.8 \mu M$
$K_{inh}$	$1.8 \mu M$	$k^+$	$1.5 \mu M^{-1} s^{-1}$
$D_{Ca}$	$16 \mu m^2 s^{-1}$	$V_{RyR}$	$0.5 s^{-1}$
$F_C$	$0.83$	$P_0$	$0.5$
$F_E$	$0.17$	$D_{NO}$	$3300 \mu m^2 s^{-1}$
$K_{NO}$	$0.09 \mu M s^{-1}$	$V_{NO}$	$0.45 \mu M$
$K_{deg}$	$0.0145 s^{-1}$		

**Fig. 1**  $[Ca^{2+}]$  distribution at different time and location instances with source influx  $\sigma = 15 \text{ pA}$  and buffer  $[B] = 5 \text{ }\mu\text{M}$



**Fig. 2** NO production flux at different time and location instances with source influx  $\sigma = 15 \text{ pA}$  and buffer  $[B] = 5 \text{ }\mu\text{M}$



concentration peaks at the source ( $x = 0 \text{ }\mu\text{m}$ ) and lowers with distant from the source and reaches the background  $[Ca^{2+}]$  levels at the other ends of neuron cells as illustrated In Fig. 1A. The reasons for  $[Ca^{2+}]$  concentration reduction

are the transport of  $[Ca^{2+}]$  ions from the source to the cell's other end, extrusion of cytosolic calcium ions by serca pump, and binding of calcium ions by buffer in neurons. In Fig. 1B, the temporal calcium enhances with time for

**Fig. 3** The NO distribution with source influx  $\sigma = 15 \text{ pA}$  and buffer  $[B] = 5 \text{ }\mu\text{M}$  at different time instants

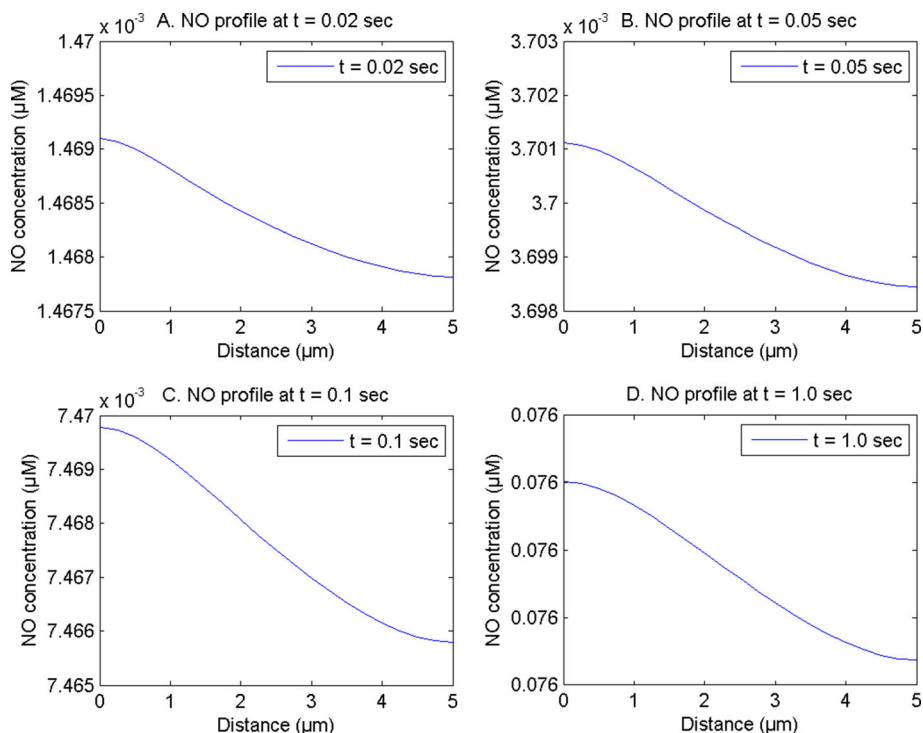
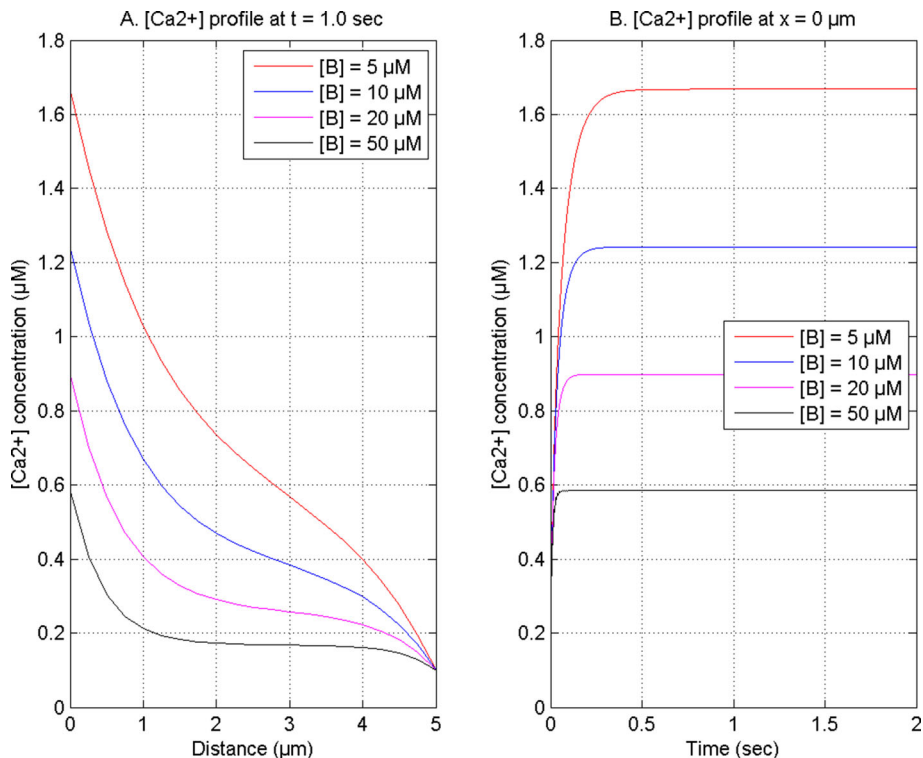


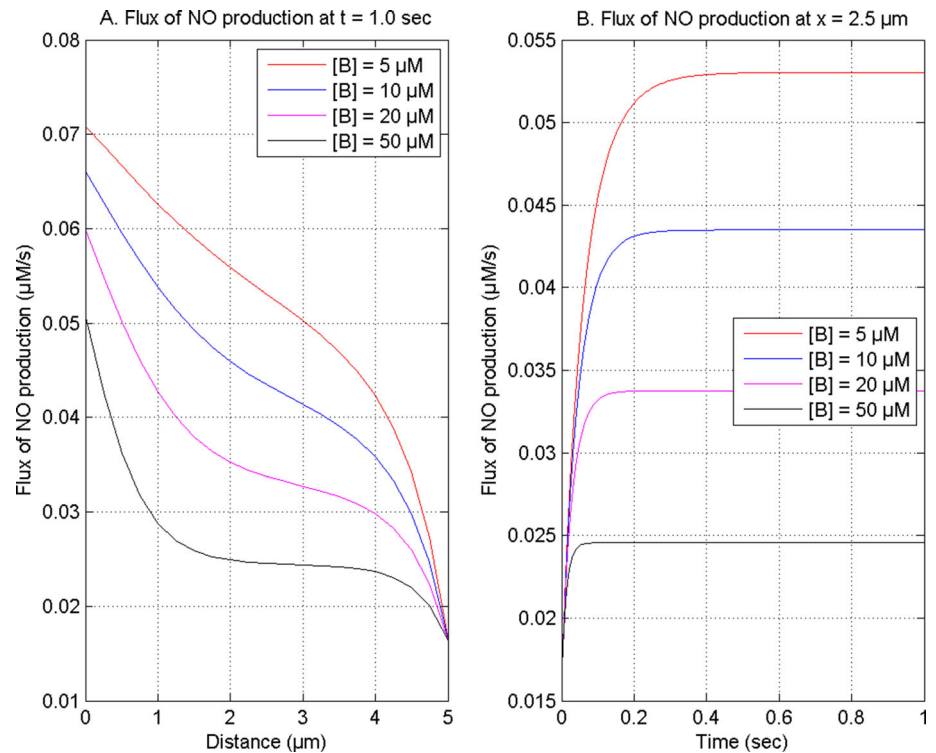
**Fig. 4**  $[\text{Ca}^{2+}]$  distribution with  $\sigma = 15 \text{ pA}$  at time  $1.0 \text{ s}$  and location  $0 \text{ }\mu\text{m}$  for various buffer amounts



various locations because calcium ions begin to release from the source channel and cytosolic calcium level increases in nerve cells. The temporal  $[\text{Ca}^{2+}]$  concentration becomes constant at time instant  $t = 0.5 \text{ s}$  for various locations (nodes) in neuron cells.

Figure 2 illustrates the spatiotemporal nitric oxide generation flux profiles at various times and locations within the nerve cell. The nitric oxide production is enhanced by the elevation in the cytosolic  $[\text{Ca}^{2+}]$  concentration due to the different processes such as calcium channels, ER

**Fig. 5** NO formation flux with  $\sigma = 15 \text{ pA}$  at time 1.0 s and location  $2.5 \text{ }\mu\text{m}$  for different buffer concentrations



mechanism, buffer, etc. in the cells. Figures 1A and 2A depict that the spatial  $[\text{Ca}^{2+}]$  and NO formation flux profile reach the peak concentration at the source and fall with distant from the source to the other side of neuron cells. In Fig. 2A, the nonlinear behavior of NO production flux reduces with time due to the decrease in the nonlinear behavior of  $[\text{Ca}^{2+}]$  concentration in Fig. 1A. The nonlinear behavior is changing with time due to elevated levels of NO by the accumulation of NO molecules and this NO accumulation is associated with elevated NO formation due to the rise in the  $[\text{Ca}^{2+}]$  concentration in neurons. In Figs. 1B and 2B, the temporal calcium and nitric oxide production flux increase with time at different nodes in neuron cells. The temporal profile of the NO production flux reaches steady-state earlier near the source position in neuron cells. Thus, this suggests that nitric oxide formation is dependent on the calcium concentration level and the dysregulation in calcium signaling leads to the dysregulation in nitric oxide production in nerve cells.

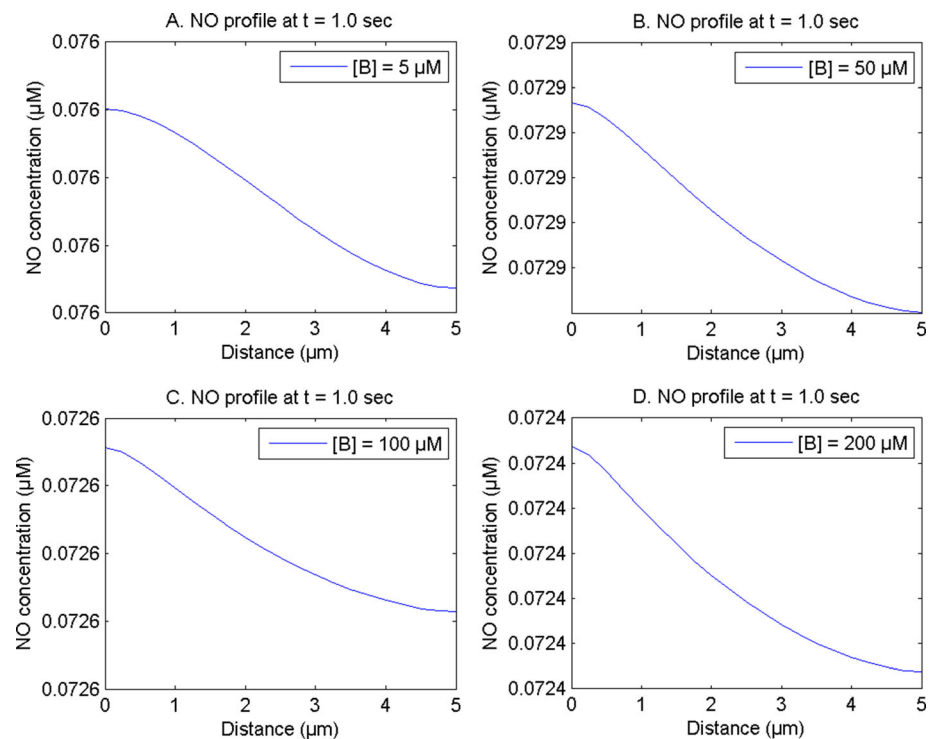
Figure 3 shows the spatial profiles of NO at varying times  $t = 0.02, 0.05, 0.1,$  and  $1.0 \text{ s}$  in nerve cells. The effects of nitric oxide diffusion, calcium-dependent NO generation, degradation on the NO distribution are noticed in Fig. 3. The spatial nitric oxide profiles attain a high concentration at source location ( $x = 0 \text{ }\mu\text{m}$ ) for different time instants in nerve cells. The NO concentration increases with time and lowers with distant positions from source location  $x = 0$  up to  $5 \text{ }\mu\text{m}$  in cells. The nitric oxide transports from the source to the other side of a neuron cell,

and its degradation is responsible for the nitric oxide reduction with distance from the source in cells.

Figure 4 exhibits the consequences of buffer concentration on neuronal  $[\text{Ca}^{2+}]$  distribution at  $t = 1.0 \text{ s}$  and location  $x = 0 \text{ }\mu\text{m}$ . The buffer mechanism is quite effective in regulating calcium concentration in neuron cells. In Fig. 4A, B the calcium concentration is falling down as buffer values elevate in nerve cells due to the binding of the additional calcium ions by the buffer, which decreases the cytosolic  $[\text{Ca}^{2+}]$  concentration in nerve cells. In Fig. 4A, the  $[\text{Ca}^{2+}]$  concentration falls spatially from  $x = 0$  up to  $5 \text{ }\mu\text{m}$  and accomplishes a peak value at the source in nerve cells. The temporal  $[\text{Ca}^{2+}]$  rises with time and reaches an equilibrium state earlier with higher buffer concentration amounts in neuron cells. The results in Fig. 4 suggest that the calcium concentration and buffer are inversely related and the calcium signaling is either balkanized or becomes less effective due to the increase in buffer concentration.

Figure 5 shows the influences of buffer concentration on the spatiotemporal neuronal NO formation flux at  $t = 1.0 \text{ s}$  and location  $x = 2.5 \text{ }\mu\text{m}$ . The role of the buffer mechanism in NO production is associated with calcium diffusion as well as ER handling through calcium release and uptake in neuron cells. In Figs. 4A and 5A, the spatial calcium and NO production flux reduce with the addition in the buffer amount in neuron cells. The elevated  $[\text{Ca}^{2+}]$  concentration due to the lower amounts of the buffer increases NO production with time, which further leads to the NO molecules

**Fig. 6** The NO distribution with  $\sigma = 15$  pA at  $t = 1.0$  s for different buffer concentrations



accumulation in neuron cells. This nitric oxide accumulation can cause the changes in nonlinear behavior of NO production in neurons illustrated in Fig. 5A. The temporal  $[\text{Ca}^{2+}]$  and NO formation flux profiles elevate with time and become constant sooner for higher buffer values in neuron cells, which is exhibited in Figs. 4B and 5B. Thus, it can be concluded that the buffer concentration regulates NO production through the calcium mechanism in nerve cells.

Figure 6 exhibits the impacts of buffer on the spatial NO profiles at  $t = 1.0$  s in nerve cells. The removal of calcium from the cytosol by EGTA buffer can reduce nitric oxide generation in cells. The nitric oxide concentration reduces as the buffer concentration increases in the cell since the nitric oxide production is regulated by the buffer via the calcium process in neuron cells. Thus, this suggests that the nitric oxide concentration level in nerve cells is dependent on the calcium concentration. In the present case, the variation of nitric oxide from 0.076 to 0.072  $\mu\text{M}$  amounts to a difference percentage of 5.26, which is a substantial change and may be within the tolerance limit of the cell. Figure 6 gives us the idea that the increase in the buffer values above 200  $\mu\text{M}$  will bring more than a 5% change in nitric oxide profiles leading to more and more neurotoxic levels.

Figure 7 depicts the impacts of source influx on the neuronal  $[\text{Ca}^{2+}]$  distribution for  $t = 1.0$  s and location  $x = 0 \mu\text{m}$ . The neuronal calcium concentration rises with the enhancement in the source influx amount from 5 to 15

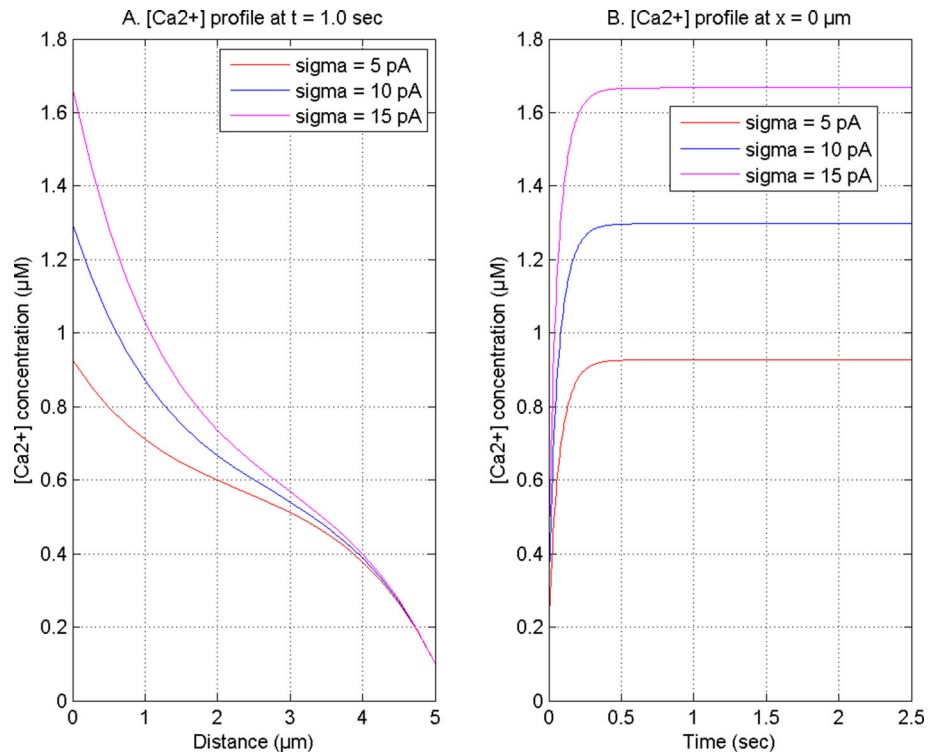
pA, since with the opening of the source channel, the  $[\text{Ca}^{2+}]$  ions release and cytosolic  $[\text{Ca}^{2+}]$  concentration elevates in nerve cells as illustrated in Fig. 7. The temporal calcium profiles achieve an equilibrium state simultaneously at  $t = 0.5$  s for varying source influx amounts in nerve cells. Thus, this indicates that the  $[\text{Ca}^{2+}]$  concentration is directly proportional to source influx in the cell and it can be crucial in the increase or decrease of calcium concentration in nerve cells.

Figure 8 shows the effects of calcium source influx on the neuronal NO formation for  $t = 1.0$  s and location  $x = 0 \mu\text{m}$ . The enhancement in calcium influx elevates the expression of NO synthase, which produces the NO in the cell. In Figs. 7, 8, the spatiotemporal calcium and nitric oxide production flux profiles elevate as the source influx values increase in nerve cells. Thus, this suggests that the consequence of source influx on the  $[\text{Ca}^{2+}]$  mechanism is transferred to the NO formation in nerve cells. Also, the required level of NO concentration can be achieved by the source influx via the calcium process in neurons.

Figure 9 shows the effects of  $[\text{Ca}^{2+}]$  source influx on the NO distribution at  $t = 0.1$  s in neuron cells. The calcium concentration increases due to the calcium influx, which produces the NO and enhances the accumulation of NO in cells. The nitric oxide concentration enhances as the calcium influx of the source elevates from 5 to 15 pA in nerve cells. Thus, this suggests that the  $[\text{Ca}^{2+}]$  influx regulates the nitric oxide signaling and acknowledges the dependence of NO on  $[\text{Ca}^{2+}]$  dynamics in nerve cells.



**Fig. 7**  $[Ca^{2+}]$  distribution with  $[B] = 5 \mu M$  for various source influx amounts at time 1.0 s and location  $0 \mu m$



**Fig. 8** NO formation flux with  $[B] = 5 \mu M$  at time 1.0 s and location  $0 \mu m$  for different source influx amounts

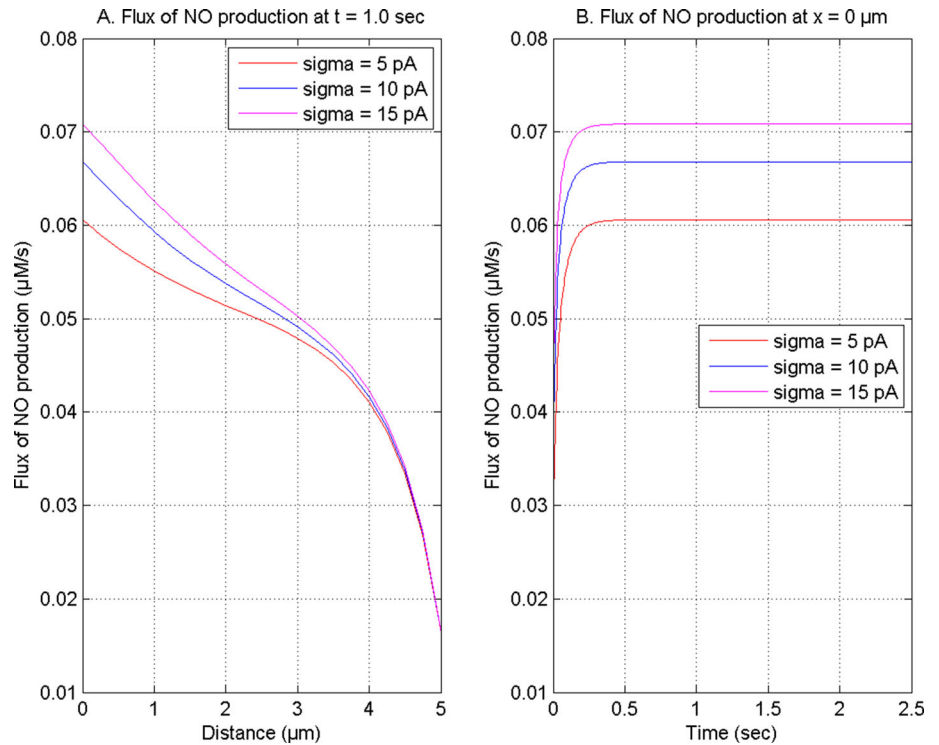
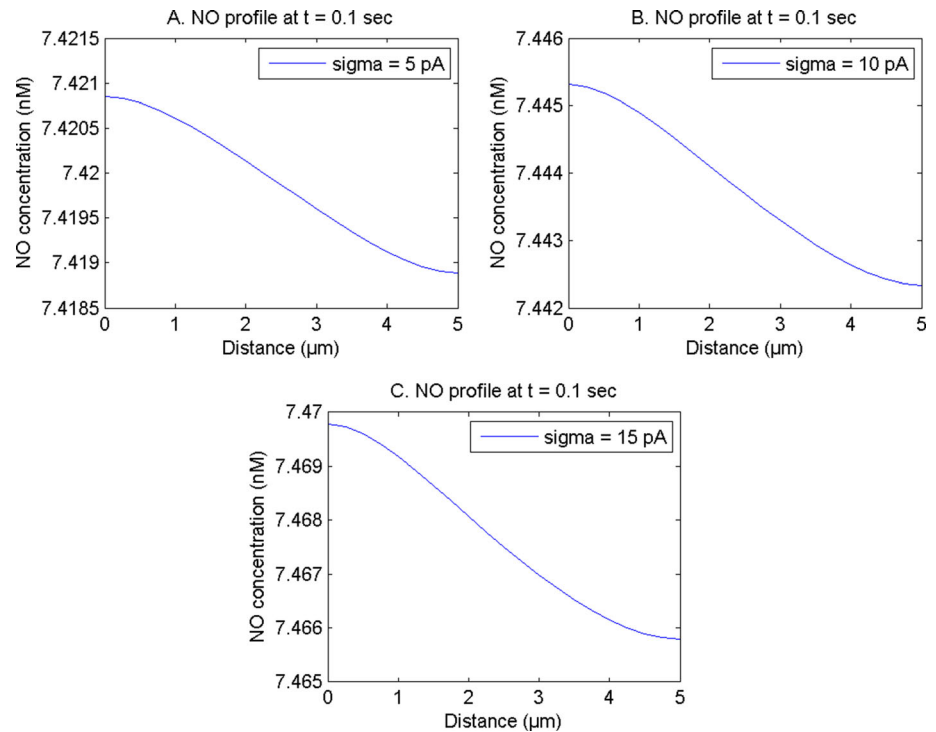


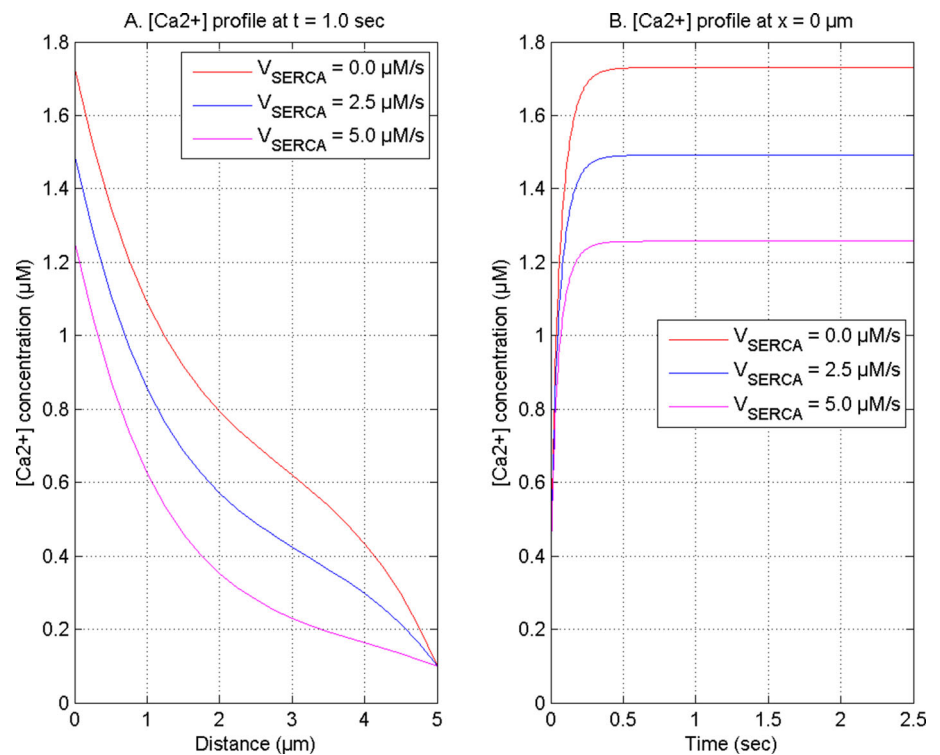
Figure 10 exhibits the impacts of the serca pump on the spatiotemporal neuronal  $[Ca^{2+}]$  distribution for  $t = 1.0$  s and location  $x = 0 \mu m$ . The serca pump acts as an ion transporter; it recharges the endoplasmic reticulum (ER) and lowers down the calcium levels to baseline levels in

neuron cells. The expression of calcium signaling in terms of bistability can be achieved by the interactions of  $IP_3$ -receptor or calcium channels with serca pump without any interaction with  $IP_3$  dynamics in cells. In Fig. 10, the spatiotemporal  $[Ca^{2+}]$  concentration profiles fall as the

**Fig. 9** NO distribution for different source influx amounts with  $[B] = 5 \mu\text{M}$  at  $t = 0.1 \text{ s}$



**Fig. 10**  $[\text{Ca}^{2+}]$  distribution with source influx  $\sigma = 15 \text{ pA}$  and buffer  $[B] = 5 \mu\text{M}$  at time 1.0 s and location  $0 \mu\text{m}$  for distinct serca pump rates



serca pump rate rises in nerve cells because the pump extrudes the additional cytosolic  $[\text{Ca}^{2+}]$  ions to ER in neuron cells. The nonlinear behavior of calcium concentration changes due to the accumulation of calcium ions in the case when the serca pump is closed in neuron cells

shown in Fig. 10A. The temporal calcium profiles increase with the passage of time and accomplish a steady state simultaneously at different serca pump rate in neurons. Thus, it can be concluded that the serca pump rate maintains the calcium at required levels in nerve cells.

**Fig. 11** NO formation flux with source influx  $\sigma = 15$  pA and buffer  $[B] = 5$   $\mu\text{M}$  at time 1.0 s and location 2.0  $\mu\text{m}$  for distinct serca pump rates

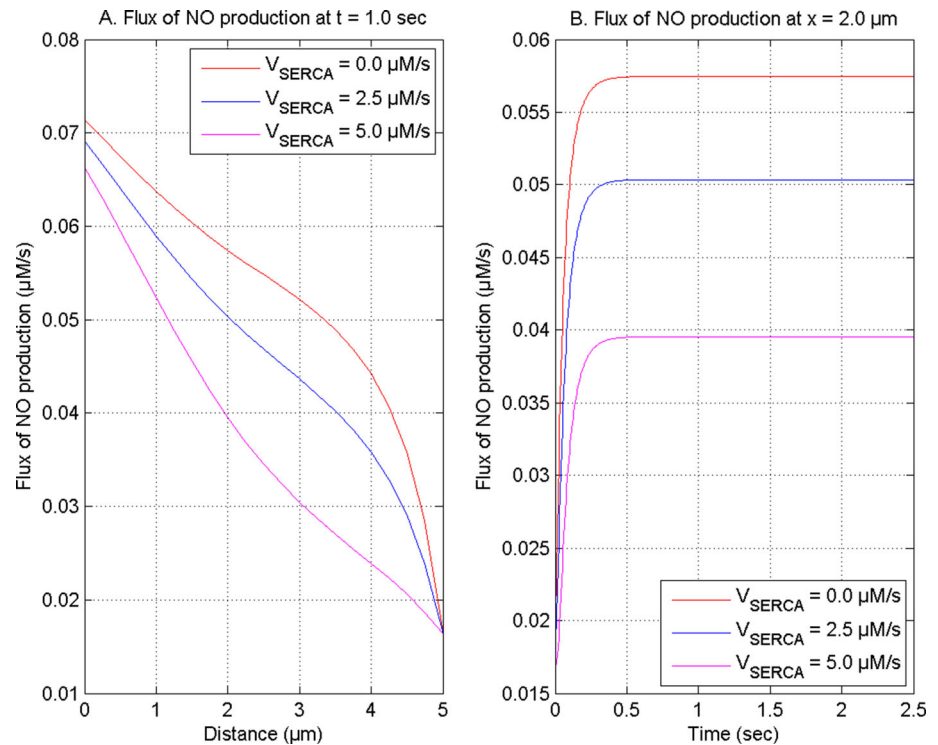


Figure 11 shows the consequences of serca pump on NO generation flux for  $t = 1.0$  s and location  $x = 2.0$   $\mu\text{m}$  in neuron cells. In Figs. 10 and 11, the calcium and nitric oxide production flux reduce spatiotemporally as the pump rate enhances in nerve cells. Also, the  $[\text{Ca}^{2+}]$  concentration and nitric oxide generation flux attain the peak value near source location in the case when the serca pump is blocked in neurons. In Fig. 11A, the changes in nonlinear behavior of NO production flux are associated with the accumulation of NO molecules by elevated calcium concentration in Fig. 10A, when the serca pump is closed in neuron cells. Thus, this implies that the serca pump affects the NO formation through the  $[\text{Ca}^{2+}]$  mechanism in neuron cells. The serca pump activities can be pivotal in the regulation of  $[\text{Ca}^{2+}]$ -dependent overproduction of nitric oxide in neuron cells and any dysregulation in the processes of the serca pump can lead to alterations in the NO distribution in neurons.

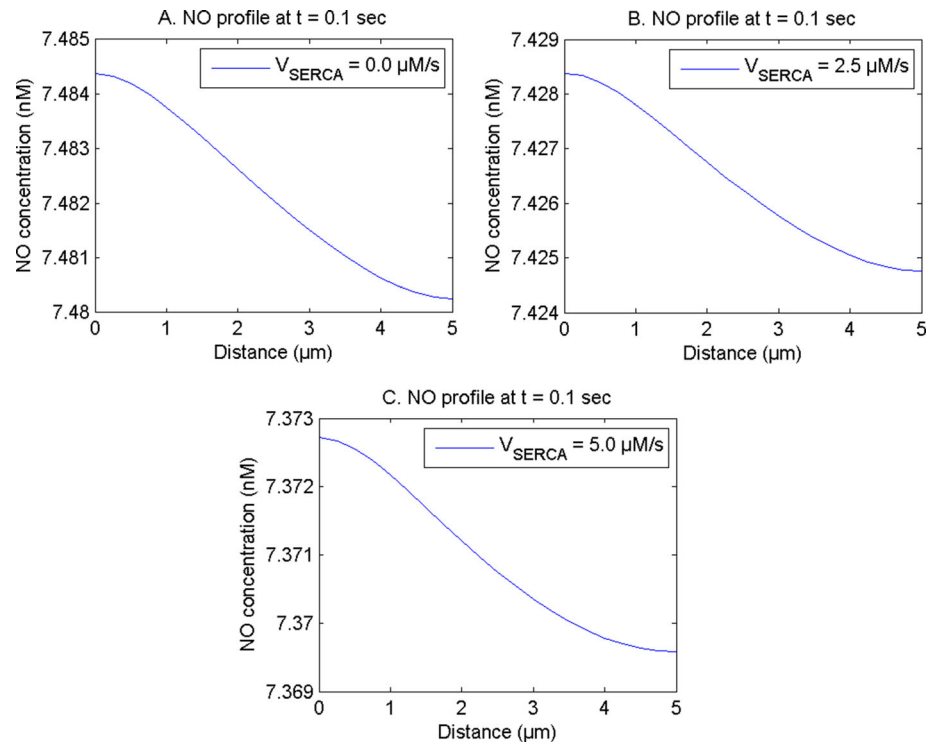
The influence of  $[\text{Ca}^{2+}]$ -based parameters on the nitric oxide concentration profile validates the dependence of NO on  $[\text{Ca}^{2+}]$  concentration in nerve cells. Figure 12 exhibits the serca pump effects on the spatial NO concentration in neuron cells at  $t = 0.1$  s. The nitric oxide concentration attains a peak value when the serca pump is not considered in nerve cells. The nitric oxide concentration reduces as the serca pump rate enhances in nerve cells. Thus, the processes of the serca pump have an effect on the NO level in nerve cells. The altered ER mechanisms can promote the

improper accumulation of nitric oxide through the disturbances in the cytosolic calcium levels in nerve cells.

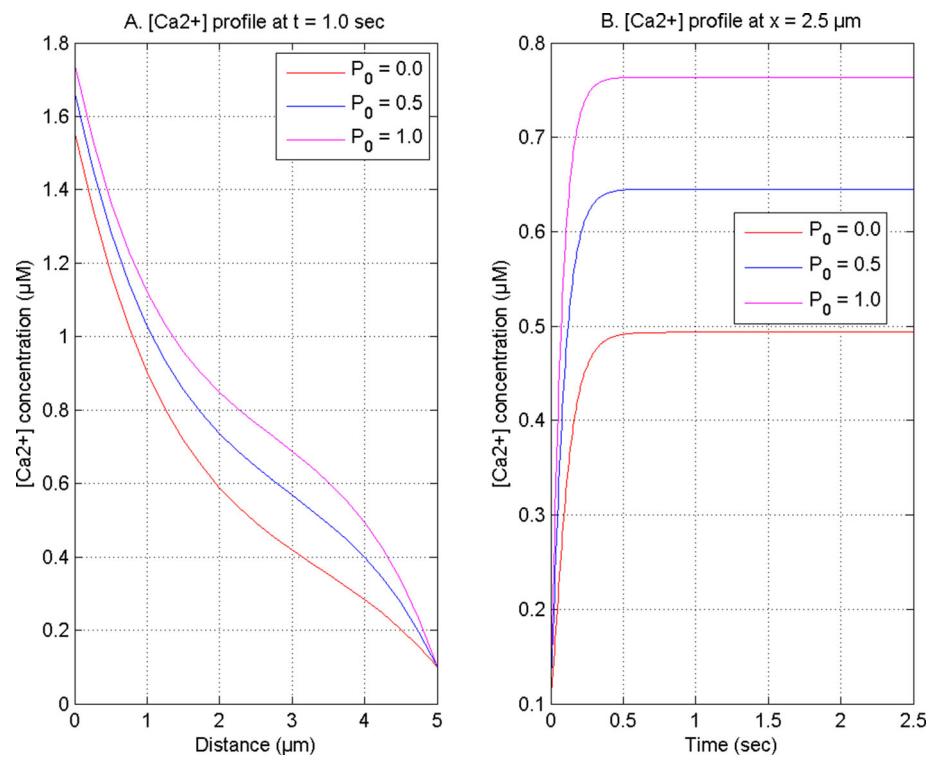
Figure 13 displays the ryanodine receptor effects on the spatiotemporal neuronal  $[\text{Ca}^{2+}]$  concentration for  $t = 1.0$  s and  $x = 2.5$   $\mu\text{m}$ . The elevation in  $[\text{Ca}^{2+}]$  levels is caused by the calcium-mediated  $[\text{Ca}^{2+}]$  release from ER, which is regulated by the activation of the ryanodine receptor in neuron cells. In Fig. 13, the calcium levels are more elevated when the ryanodine receptor is fully activated ( $P_0 = 1$ ) in cells. The calcium profiles attain the minimum concentration when the ryanodine receptor is fully closed ( $P_0 = 0$ ) in neuron cells. In Fig. 13A, the calcium concentration reduces spatially from source location and accomplishes the background calcium level (0.1  $\mu\text{M}$ ) in neurons for different ryanodine receptor states. Also, the variation in nonlinear behavior of  $[\text{Ca}^{2+}]$  concentration in Fig. 13A is associated with the accumulation of  $[\text{Ca}^{2+}]$  ions in neurons. The accumulation of neuronal calcium ions is elevated in the case of a completely open ryanodine receptor. In Fig. 13B, the temporal calcium distribution enhances with time and attains the equilibrium state simultaneously at  $t = 0.5$  s for different ryanodine receptor states in neurons.

Figure 14 illustrates the influences of the ryanodine receptor on the spatiotemporal neuronal NO production flux for  $t = 1.0$  s and location  $x = 2.5$   $\mu\text{m}$  in neuron cells. The elevation in cytosolic  $[\text{Ca}^{2+}]$  concentration in nerve cells through calcium channels produces nitric oxide through the binding of neuronal NO synthase. In Figs. 13

**Fig. 12** NO concentration with source influx  $\sigma = 15$  pA and buffer  $[B] = 5$   $\mu\text{M}$  at  $t = 0.1$  s for different serca pump rates



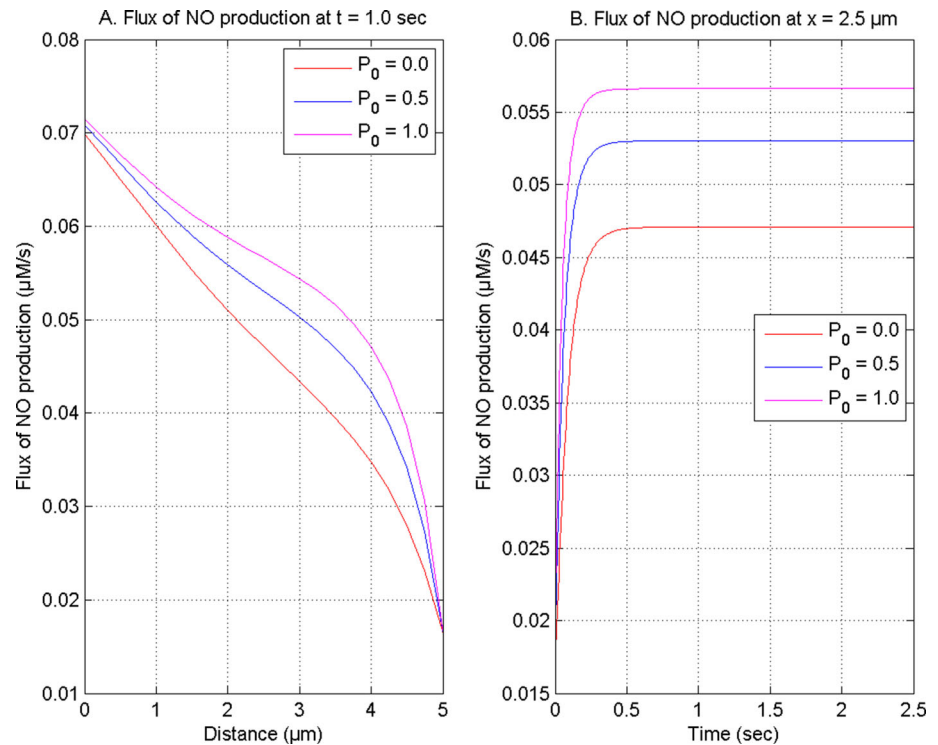
**Fig. 13**  $[\text{Ca}^{2+}]$  concentration with source influx  $\sigma = 15$  pA and buffer  $[B] = 5$   $\mu\text{M}$  at time 1.0 s and location 2.5  $\mu\text{m}$  for different ryanodine receptor states



and 14, the spatiotemporal calcium and nitric oxide production flux are more elevated for the fully active

( $P_0 = 1.0$ ) state of the ryanodine receptor than for the partially active ( $P_0 = 0.5$ ) and fully inactive ( $P_0 = 0$ )

**Fig. 14** The NO formation flux with source influx  $\sigma = 15$  pA and buffer  $[B] = 5$   $\mu\text{M}$  at time 1.0 s and location  $2.5$   $\mu\text{m}$  for different ryanodine receptor states



ryanodine receptor states in a neuron cell. In Figs. 13A and 14A, the spatial calcium and nitric oxide production flux profiles reduce with distance for various ryanodine receptor states in nerve cells. The temporal calcium and nitric oxide production flux profiles increase with time and become constant for different ryanodine receptor states in neurons, which is exhibited in Figs. 13B and 14B. Thus, this suggests that different ryanodine receptor states affect the NO formation through the calcium process in nerve cells.

Figure 15 illustrates the effects of the ryanodine receptor on nitric oxide distributions at time  $t = 0.1$  s in neuron cells. The interaction of ER handling through the ryanodine receptor and calcium concentration can lead to the activation of NO synthase in the cell. When the ryanodine receptor is entirely open ( $P_0 = 0.5$ ), the nitric oxide concentration profiles are more elevated than the partially active ( $P_0 = 0.5$ ) and fully closed ( $P_0 = 0$ ) cases of the ryanodine receptor in the nerve cell. Thus, Figs. 13 and 15 imply that the ryanodine receptor affects the  $[\text{Ca}^{2+}]$  and NO levels, which acknowledges the  $[\text{Ca}^{2+}]$  and NO cooperation in neuron cells.

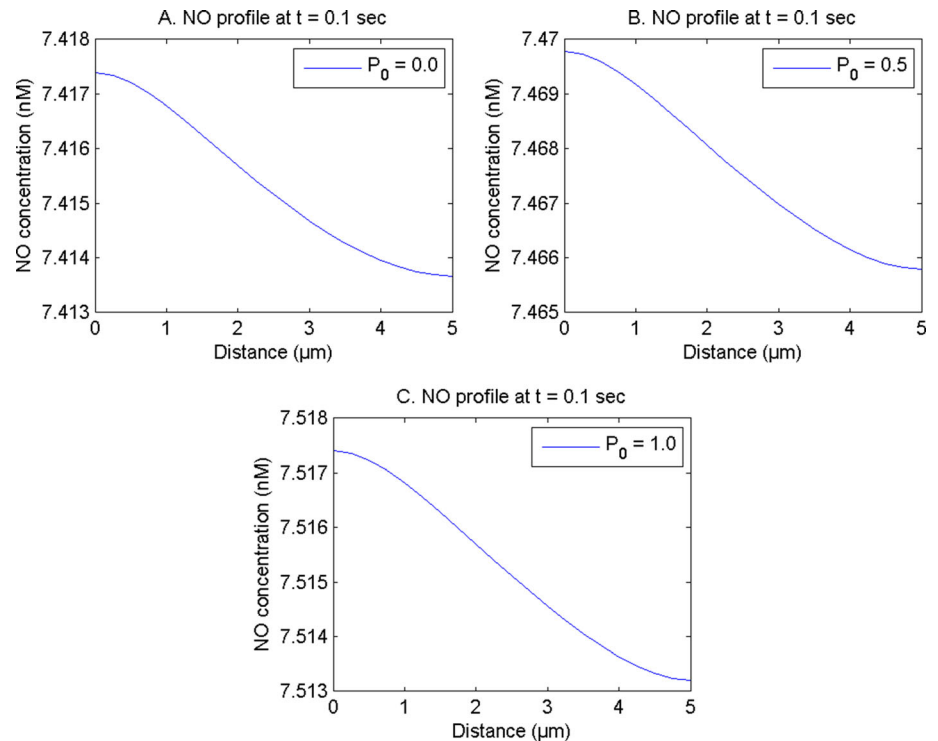
Figure 16 displays the impacts of  $\text{IP}_3$  concentration on the spatial  $[\text{Ca}^{2+}]$  and NO generation flux at location  $x = 2.0$   $\mu\text{m}$  in neuron cells. The transition in the calcium from low to high states is accomplished by the interaction of calcium with the  $\text{IP}_3$  receptor as it is initiated by the significant elevation in calcium or  $\text{IP}_3$  concentration in neuron cells. The calcium concentration is regulated by the  $\text{IP}_3$  receptor as it releases  $[\text{Ca}^{2+}]$  from ER to cytosol in

neuron cells. In Fig. 16A, the calcium concentration rises as the  $\text{IP}_3$  concentration elevates in nerve cells. The nitric oxide formation flux also enhances with the rise in the  $\text{IP}_3$  concentration in neurons illustrated in Fig. 16B. Thus, this suggests that the  $\text{IP}_3$  levels affect the  $[\text{Ca}^{2+}]$  concentration as well as nitric oxide formation in nerve cells. Also, the required levels of cytosolic calcium can be accomplished by  $\text{IP}_3$ -induced calcium release in neuron cells for proper execution of various cellular processes.

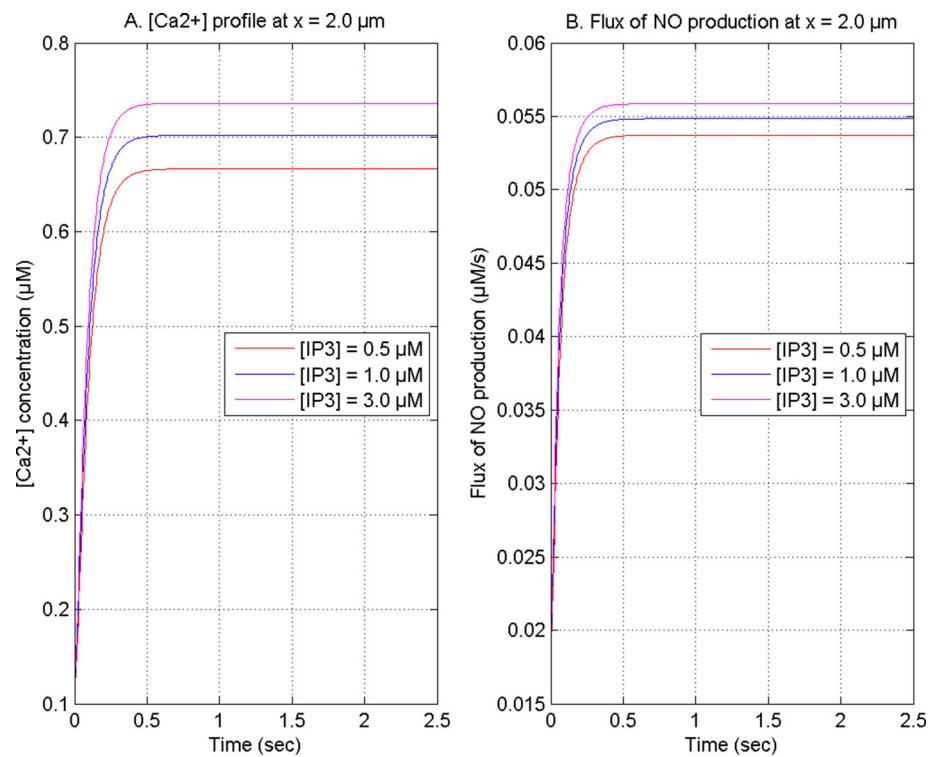
Figure 17 shows the influences of  $\text{IP}_3$  concentration level on the spatial nitric oxide distribution at  $t = 0.1$  s in nerve cells. The  $\text{IP}_3$ -receptor mediated calcium signaling is also responsible for the NO synthase activation and NO generation in cells. The concentration of nitric oxide elevates as the  $\text{IP}_3$  concentration level rises since the nitric oxide formation is dependent on the  $[\text{Ca}^{2+}]$  levels in nerve cells. Thus, this suggests that the  $\text{IP}_3$  concentration regulates the  $[\text{Ca}^{2+}]$  and NO concentration levels in nerve cells. The dysregulation in the  $\text{IP}_3$  concentration level can cause the alteration in  $[\text{Ca}^{2+}]$  and NO signaling in nerve cells.

Figure 18 exhibits the influences of higher buffer concentrations on the temporal  $[\text{Ca}^{2+}]$  distribution at position  $x = 0$   $\mu\text{m}$  in neuron cells. The calcium concentration lowers with the rise in the buffer values since the buffer fixes additional cytosolic  $[\text{Ca}^{2+}]$  ions and reduces the  $[\text{Ca}^{2+}]$  concentration in neurons. For higher buffer values, the calcium profiles show the oscillations in the initial time and accomplish the equilibrium state at the earliest possible time in nerve cells. The reasons behind the oscillatory

**Fig. 15** Nitric oxide (NO) profiles with  $[B] = 5 \mu\text{M}$  and  $\sigma = 15 \text{ pA}$  at time  $0.1 \text{ s}$  for different states of ryanodine receptor



**Fig. 16**  $[\text{Ca}^{2+}]$  concentration and NO production flux with buffer  $[B] = 5 \mu\text{M}$  and source influx  $\sigma = 15 \text{ pA}$  at  $x = 2.0 \mu\text{m}$  for different  $\text{IP}_3$  concentrations



behavior of  $[\text{Ca}^{2+}]$  concentration are that the buffer decreases the calcium concentration and other mechanisms of calcium dynamics try to elevate calcium concentration in the cell. These mismatches among the buffer process and different mechanisms of calcium signaling produce

fluctuations in the  $[\text{Ca}^{2+}]$  concentration in neurons. The rapid equilibration mechanism of calcium can be explained by the sequestration of cytosolic calcium ions by the higher buffer concentration in neuron cells.

**Fig. 17** NO concentration with  $[B] = 5 \mu\text{M}$  and  $\sigma = 15 \text{ pA}$  at time  $0.1 \text{ s}$  for different  $\text{IP}_3$  concentrations

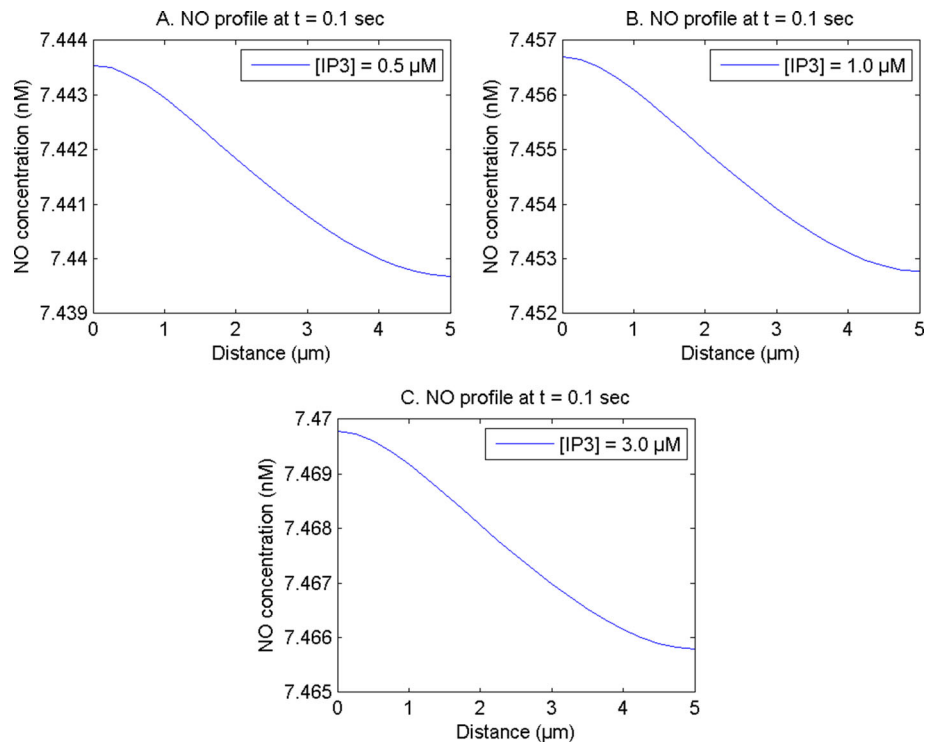


**Fig. 18**  $[\text{Ca}^{2+}]$  distribution with  $\sigma = 15 \text{ pA}$  at  $x = 0 \mu\text{m}$  for different buffer amounts

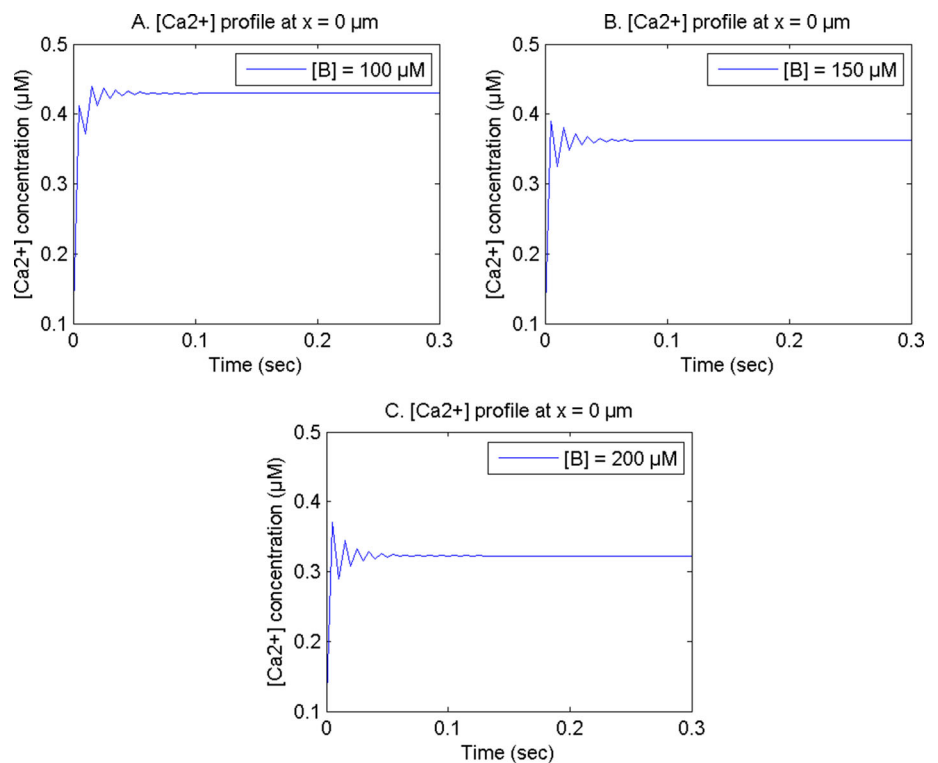
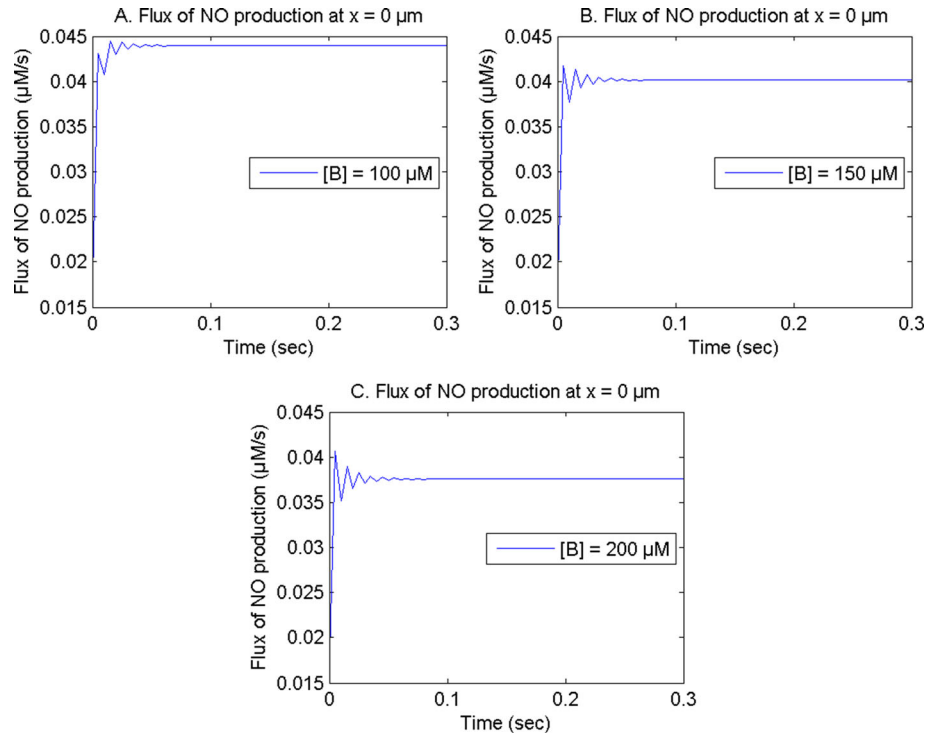


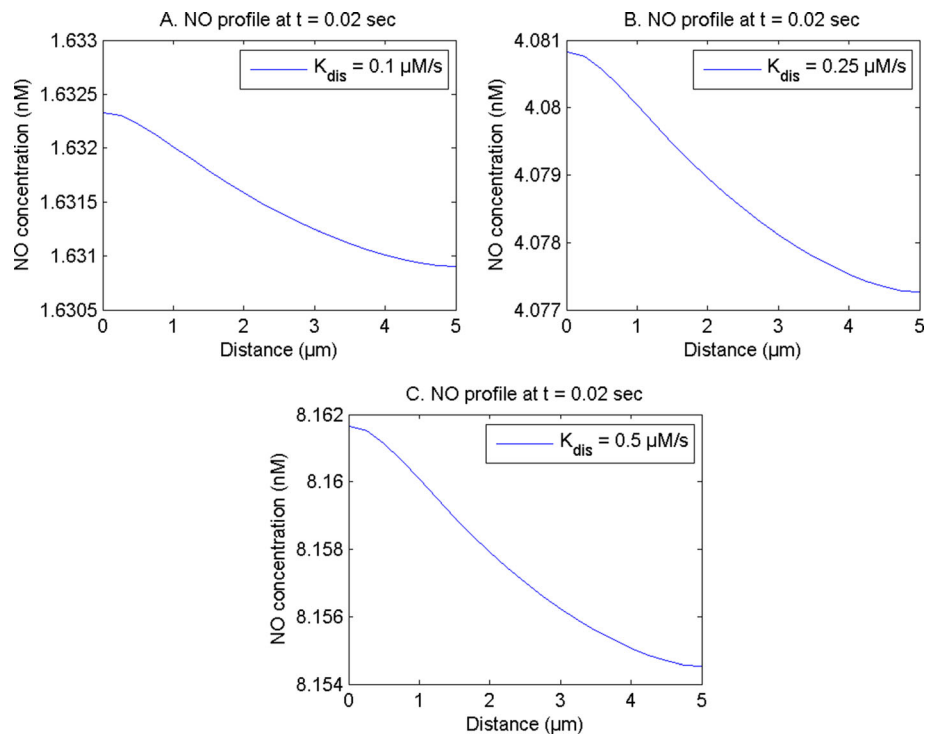
Figure 19 illustrates the consequences of higher buffer concentration values on the temporal NO production flux at location  $x = 0 \mu\text{m}$  in neuron cells. In Figs. 18 and 19, the temporal calcium concentration and NO production flux exhibit oscillatory behavior in the initial period and attain

the steady-state in neuron cells. Thus, this suggests that the dysregulation in the  $[\text{Ca}^{2+}]$  signaling can be described as the association-disassociation equilibrium is significantly rapid due to the influence of buffer concentration on the rapid sequestering of  $[\text{Ca}^{2+}]$  ions in neurons, which can

**Fig. 19** The NO production flux with  $\sigma = 15$  pA at  $x = 0$   $\mu\text{m}$  for different buffer values



**Fig. 20** Nitric oxide concentration with  $[B] = 5$   $\mu\text{M}$  and  $\sigma = 15$  pA at  $t = 0.02$  s



further lead to the disturbances in the NO production in nerve cells.

Figure 20 displays the nitric oxide distribution for different NO production rates at  $t = 0.02$  s in nerve cells. The nitric oxide concentration rises as the nitric oxide production rate in neuron cells increases. Also, the nitric oxide

concentration lowers with distant from  $x = 0$   $\mu\text{m}$  to the other side of nerve cells. The higher production, as well as accumulation and improper clearance of NO in the cell may cause neurotoxicity causing different types of diseases.



**Table 2** Error analysis for  $[Ca^{2+}]$  distribution at  $x = 0 \mu m$

Time (s)	E = 20	E = 40	Absolute relative error	Percentage of error
0.1	1.383130650985767	1.380245892332146	0.0029	0.21%
0.2	1.591873596197453	1.592473831707585	0.00060024	0.037692%
0.5	1.665900866929962	1.667338407127080	0.0014	0.083966%
1.0	1.667445337701081	1.668893705194334	0.0014	0.083888%

**Table 3** Error analysis for NO distribution at  $x = 0 \mu m$

Time (s)	E = 20	E = 40	Absolute relative error	Percentage of error (%)
0.1	0.007469781539798	0.007469844139095	$6.2599 \times 10^{-8}$	0.000838
0.2	0.015091125700428	0.015091265947851	$1.4025 \times 10^{-7}$	0.000929
0.5	0.038032909169583	0.038033268484400	$3.5931 \times 10^{-7}$	0.000944
1.0	0.076004041756498	0.076004763744077	$7.2199 \times 10^{-7}$	0.000949

**Table 4** Calcium concentrations compared with Wagner et al. (2004) at  $t = 50 s$

Distance ( $\mu m$ )	Calcium concentration (Wagner et al. 2004)	Calcium concentration (present outcomes)
$x = 0.0 \mu m$	1.350000000000000	1.350247965091095
$x = 1.0 \mu m$	1.193112370933056	1.185408770297697
$x = 2.0 \mu m$	1.016157013638407	1.004580670612548
$x = 3.0 \mu m$	0.795857981478567	0.784116110251518
$x = 4.0 \mu m$	0.503271331553075	0.495184121811449
$x = 5.0 \mu m$	0.100000000000000	0.100000000000000

Where, the number of elements is denoted by E. The absolute relative errors and error percentages for  $[Ca^{2+}]$  and NO in neurons are given respectively in Tables 2 and 3. For time 0.1, 0.2, 0.5, and 1.0 s, the model accuracy for  $[Ca^{2+}]$  is sequentially 99.79%, 99.962308%, 99.916034%, 99.916112%, and model accuracy for NO dynamics is respectively 99.999162%, 99.999071%, 99.999056%, and 99.999051%. Thus, for the present model, the highest error % and lowest accuracy are respectively 0.21% and 99.79%. Very low grid sensitivity suggests that the solution is independent of the grid.

For stability analysis, when the spectral radius is unity or less, the system is deemed to be stable (Öziş et al. 2003). The spectral radius in the present case was 0.9999 (less than 1). As a result, the finite element approach utilized in the present condition yields a stable solution.

The numerically obtained  $[Ca^{2+}]$  and NO concentrations at buffer  $[B] = 0 \mu M$ ,  $P_0 = 0$ , and  $\sigma = 2.625 pA$ , and on  $[Ca^{2+}]$  profile, and  $IP_3$  concentration as  $3.0 \mu M$ , and the obtained findings are comparable with previously published outcomes of Wagner et al. (2004) for time instant (50 s), and the findings are all in agreement as illustrated in Table 4. Moreover, no experiment outcomes are available for additional validation of the  $[Ca^{2+}]$  and NO dynamics acquired results, but the findings are consistent with biological facts.

## Conclusion

The disorders in the regulatory spatiotemporal neurodynamics of calcium and nitric oxide are examined effectively and successfully using a model that is constructed using the finite element technique. The alterations in the diverse processes such as buffer, serca pump, ryanodine receptor, source influx, etc. can cause disorders in the regulatory spatiotemporal  $[Ca^{2+}]$  and NO dynamics in neuron cells. The high amounts of serca pump rate, source influx, and buffer, low amounts of serca pump and buffer as well as entirely open ryanodine receptor state can lead to the dysregulation in the spatiotemporal neurodynamics of calcium and nitric oxide. The effect of alterations in these processes was noticed on the dynamics of  $[Ca^{2+}]$  and nitric oxide and also on the NO production in nerve cells. The following novel conclusions are drawn from the findings,

- i. For low amounts of the serca pump rate and buffer and high amounts of source influx, the  $[Ca^{2+}]$  concentration gets elevated, which in turn enhances the NO production and nitric oxide concentration in nerve cells. The elevated nitric oxide concentration in nerve cells is associated with Parkinson’s disease (Zhang et al. 2006).

- ii. The high buffer values cause the disturbances in form of fluctuations in the  $[Ca^{2+}]$  concentration, which leads to fluctuations in the NO production in neuron cells. Thus, the disturbances in nitric oxide production can cause the inappropriate accumulation of nitric oxide in nerve cells, which is associated with cerebral ischemia (Huang 2004), trauma, and chronic epilepsy (Cherian et al. 2004).
- iii. The elevated  $IP_3$  concentration causes the elevation in  $[Ca^{2+}]$  concentration, which further elevates the NO synthesis as well as nitric oxide accumulation in nerve cells.
- iv. The elevated calcium concentration due to the entirely open ryanodine receptor state increases the NO production and nitric oxide accumulation in neuron cells. The alterations in the ryanodine functioning can cause Alzheimer’s disease (Brini et al. 2014) and Familial hemiplegic migraine (FHM) in neurons.

Thus, one can conclude that the alterations in the source influx, serca pump, ryanodine receptor, buffer, and  $IP_3$  mechanisms can cause the disorders in the regulatory spatiotemporal neurodynamics of calcium and nitric oxide, which can lead to neurotoxicity causing Parkinson’s disease, chronic epilepsy, trauma, cerebral ischemia, etc. The finite element technique is effective in determining the solution to provide crucial information on the consequences of the different altered parameters on the regulation and dysregulation of the spatiotemporal neurodynamics of calcium and nitric oxide and their association with various neuronal diseases. The crucial information about the range of alterations in parameters and their consequential magnitude and intensity of disorders in neuronal dynamics generated in this study can be useful for therapeutic applications. This model can be advanced further to explore the calcium and nitric oxide dynamics under the disease affected circumstances for Parkinson’s disease, trauma, chronic epilepsy, cerebral ischemia, etc. in neuron cells.

### Appendix: Model equations description

For each element, the shape functions of  $[Ca^{2+}]$  and NO are considered as,

$$u^{(e)} = q_1^{(e)} + q_2^{(e)} x, \tag{18}$$

$$v^{(e)} = r_1^{(e)} + r_2^{(e)} x, \tag{19}$$

$$u^{(e)} = S^T q^{(e)}, v^{(e)} = S^T r^{(e)}, \tag{20}$$

$$S^T = [1 \ x], q^{(e)T} = [q_1^{(e)} \ q_2^{(e)}], r^{(e)T} = [r_1^{(e)} \ r_2^{(e)}], \tag{21}$$

Incorporating nodal conditions in Eq. (20), we have

$$\bar{u}^{(e)} = S^{(e)} q^{(e)}, \bar{v}^{(e)} = S^{(e)} r^{(e)}, \tag{22}$$

where,

$$\bar{u}^{(e)} = \begin{bmatrix} u_i \\ u_j \end{bmatrix}, \bar{v}^{(e)} = \begin{bmatrix} v_i \\ v_j \end{bmatrix}, \text{ and } S^{(e)} = \begin{bmatrix} 1 & x_i \\ 1 & x_j \end{bmatrix}, \tag{23}$$

By the Eq. (22), we get

$$q^{(e)} = R^{(e)} \bar{u}^{(e)}, r^{(e)} = R^{(e)} \bar{v}^{(e)}, \tag{24}$$

and

$$R^{(e)} = S^{(e)-1}, \tag{25}$$

From Eq. (24), placing  $q^{(e)}$  and  $r^{(e)}$  in (20), we have

$$u^{(e)} = S^T R^{(e)} \bar{u}^{(e)}, v^{(e)} = S^T R^{(e)} \bar{v}^{(e)}, \tag{26}$$

Discretized form of Eq. (1 and 8) is provided by,

The integrals  $I_1^{(e)}$  and  $I_2^{(e)}$  can be represented as,

$$I_1^{(e)} = I_{a1}^{(e)} - I_{b1}^{(e)} + I_{c1}^{(e)} - I_{d1}^{(e)} + I_{e1}^{(e)} + I_{f1}^{(e)} - I_{g1}^{(e)} - I_{h1}^{(e)}, \tag{27}$$

where

$$I_{a1}^{(e)} = \int_{x_i}^{x_j} \left\{ \left( \frac{\partial u^{(e)}}{\partial x} \right)^2 \right\} dx, \tag{28}$$

$$I_{b1}^{(e)} = \frac{d}{dt} \int_{x_i}^{x_j} \left[ \frac{u^{(e)}}{D_{Ca}} \right] dx, \tag{29}$$

$$I_{c1}^{(e)} = \frac{V_{IPR}}{D_{ca}F_c} \int_{x_i}^{x_j} [\alpha u^{(e)} + \gamma] dx, \tag{30}$$

$$I_{d1}^{(e)} = \frac{V_{SERCA}}{D_{ca}F_c} \int_{x_i}^{x_j} [\kappa u^{(e)} + \eta] dx, \tag{31}$$

$$I_{e1}^{(e)} = \frac{V_{LEAK}}{D_{ca}F_c} \int_{x_i}^{x_j} [[Ca^{2+}]_{ER} - u^{(e)}] dx, \tag{32}$$

$$I_{f1}^{(e)} = \frac{V_{RyR}P_0}{D_{ca}F_c} \int_{x_i}^{x_j} [[Ca^{2+}]_{ER} - u^{(e)}] dx, \tag{33}$$

$$I_{g1}^{(e)} = \frac{K^+}{D_{ca}} \int_{x_i}^{x_j} [u^{(e)} - [Ca^{2+}]_{\infty}] dx, \tag{34}$$

$$I_{h1}^{(e)} = f^{(e)} \frac{\sigma}{D_{cax=0}}, \tag{35}$$

Now,

$$I_2^{(e)} = I_{a2}^{(e)} - I_{b2}^{(e)} + I_{c2}^{(e)} - I_{d2}^{(e)}, \tag{36}$$

$$I_{a2}^{(e)} = \int_{x_i}^{x_j} \left\{ \left( \frac{\partial v^{(e)}}{\partial x} \right)^2 \right\} dx, \tag{37}$$

$$I_{b2}^{(e)} = \frac{d}{dt} \int_{x_i}^{x_j} \left[ \frac{v^{(e)}}{D_{NO}} \right] dx, \tag{38}$$

$$I_{c2}^{(e)} = \frac{V_{NO}}{D_{NO}} \int_{x_i}^{x_j} [\mu u^{(e)} + \tau] dx, \tag{39}$$

$$I_{e2}^{(e)} = \frac{K_{deg}}{D_{NO}} \int_{x_i}^{x_j} [v^{(e)}] dx, \tag{40}$$

Linearization of nonlinear coupled  $[Ca^{2+}]$  and NO dynamics yields the different parameters  $\alpha, \kappa, \gamma, \eta, \tau,$  and  $\mu$ . Analyzing the equations and including boundary conditions yields the following systems of equations,

$$\frac{dI_1}{d\bar{u}^{(e)}} = \sum_{e=1}^N \bar{Q}^{(e)} \frac{dI_1^{(e)}}{d\bar{u}^{(e)}} \bar{Q}^{(e)T} = 0. \tag{41}$$

$$\frac{dI_2}{d\bar{v}^{(e)}} = \sum_{e=1}^N \bar{Q}^{(e)} \frac{dI_2^{(e)}}{d\bar{v}^{(e)}} \bar{Q}^{(e)T} = 0. \tag{42}$$

where,

$$\bar{Q}^{(e)} = \begin{bmatrix} 0 & 0 \\ \dot{0} & \dot{0} \\ 1 & 0 \\ 0 & 1 \\ 0 & 0 \\ \cdot & \cdot \\ 0 & 0 \end{bmatrix} \text{ and } \bar{u} = \begin{bmatrix} u_1 \\ u_2 \\ u_3 \\ \cdot \\ \cdot \\ u_{19} \\ u_{20} \\ u_{21} \end{bmatrix}, \bar{v} = \begin{bmatrix} v_1 \\ v_2 \\ v_3 \\ \cdot \\ \cdot \\ v_{19} \\ v_{20} \\ v_{21} \end{bmatrix}, \tag{43}$$

$$\frac{dI_1^{(e)}}{d\bar{u}^{(e)}} = \frac{dI_{a1}^{(e)}}{d\bar{u}^{(e)}} + \frac{d}{dt} \frac{dI_{b1}^{(e)}}{d\bar{u}^{(e)}} + \frac{dI_{c1}^{(e)}}{d\bar{u}^{(e)}} - \frac{dI_{d1}^{(e)}}{d\bar{u}^{(e)}} + \frac{dI_{e1}^{(e)}}{d\bar{u}^{(e)}} + \frac{dI_{f1}^{(e)}}{d\bar{u}^{(e)}} - \frac{dI_{g1}^{(e)}}{d\bar{u}^{(e)}} - \frac{dI_{h1}^{(e)}}{d\bar{u}^{(e)}}, \tag{44}$$

$$\frac{dI_2^{(e)}}{d\bar{v}^{(e)}} = \frac{dI_{a2}^{(e)}}{d\bar{v}^{(e)}} + \frac{d}{dt} \frac{dI_{b2}^{(e)}}{d\bar{v}^{(e)}} + \frac{dI_{c2}^{(e)}}{d\bar{v}^{(e)}} - \frac{dI_{d2}^{(e)}}{d\bar{v}^{(e)}}, \tag{45}$$

$$[A]_{42 \times 42} \begin{bmatrix} \frac{\partial \bar{u}}{\partial t} \\ \frac{\partial \bar{v}}{\partial t} \end{bmatrix}_{21 \times 1} + [B]_{42 \times 42} \begin{bmatrix} \bar{u} \\ \bar{v} \end{bmatrix}_{21 \times 1} = [F]_{42 \times 1}, \tag{46}$$

Here, A and B denote the system matrices, and F represents the system vectors. In finite element technique, the Crank–Nicolson scheme is utilized for solving the time derivative.

**Author contributions** In terms of problem formulation, solution, data correction/literature review, and interpretation of the outcomes, we both the authors made equal contributions to this paper. Author (1) develops the Matlab program.

**Funding** Not available.

**Data availability** Not applicable.

**Declarations**

**Conflict of interest** The authors of this work declare that no conflicts of interest exist.

**Ethics approval** Not applicable.

**References**

Ahmed Z, Connor JA (1988) Calcium regulation by and buffer capacity of molluscan neurons during calcium transients. *Cell Calcium* 9:57–69. [https://doi.org/10.1016/0143-4160\(88\)90025-5](https://doi.org/10.1016/0143-4160(88)90025-5)

Aimi Y, Kimura H, Kinoshita T et al (1993) Histochemical localization of nitric oxide synthase in rat enteric nervous system. *Neuroscience* 53:553–560. [https://doi.org/10.1016/0306-4522\(93\)90220-A](https://doi.org/10.1016/0306-4522(93)90220-A)

Bodalia A, Li H, Jackson MF (2013) Loss of endoplasmic reticulum  $Ca^{2+}$  homeostasis: contribution to neuronal cell death during cerebral ischemia. *Acta Pharmacol Sin* 34:49–59. <https://doi.org/10.1038/aps.2012.139>

Boehning D, Snyder SH (2003) Novel neural modulators. *Annu Rev Neurosci* 26:105–131. <https://doi.org/10.1146/annurev.neuro.26.041002.131047>

Bogdan C (2001) Nitric oxide and the immune response: nature immunology. *Nat Immunol* 2:907–916

Bolotina VM, Najibi S, Palacino JJ et al (1994) Nitric oxide directly activates calcium-dependent potassium channels in vascular smooth muscle. *Nature* 368:850–853. <https://doi.org/10.1038/368850a0>

Bootman MD, Berridge MJ (1995) The elemental principles of calcium signaling. *Cell* 83:675–678. [https://doi.org/10.1016/0092-8674\(95\)90179-5](https://doi.org/10.1016/0092-8674(95)90179-5)

Bredt DS, Hwang PM, Snyder SH (1990) Localization of nitric oxide synthase indicating a neural role for nitric oxide. *Nature* 347:768–770. <https://doi.org/10.1038/347768a0>

Brenman JE, Xia H, Chao DS et al (1997) Regulation of neuronal nitric oxide synthase through alternative transcripts. *Dev Neurosci* 19:224–231. <https://doi.org/10.1159/000111211>

- Brini M, Cali T, Ottolini D, Carafoli E (2014) Neuronal calcium signaling: function and dysfunction. *Cell Mol Life Sci* 71:2787–2814. <https://doi.org/10.1007/s00018-013-1550-7>
- Brown SA, Morgan F, Watras J, Loew LM (2008) Analysis of phosphatidylinositol-4,5-bisphosphate signaling in cerebellar Purkinje spines. *Biophys J* 95:1795–1812. <https://doi.org/10.1529/biophysj.108.130195>
- Ceccatelli S, Lundberg JM, Zhang X et al (1994) Immunohistochemical demonstration of nitric oxide synthase in the peripheral autonomic nervous system. *Brain Res* 656:381–395. [https://doi.org/10.1016/0006-8993\(94\)91483-4](https://doi.org/10.1016/0006-8993(94)91483-4)
- Cherian L, Hlatky R, Robertson CS (2004) Nitric oxide in traumatic brain injury. *Brain Pathol* 14:195–201. <https://doi.org/10.1111/j.1750-3639.2004.tb00053.x>
- Chung JW, Ryu WS, Kim BJ, Yoon BW (2015) Elevated calcium after acute ischemic stroke: association with a poor short-term outcome and long-term mortality. *J Stroke* 17:54–59. <https://doi.org/10.5853/jos.2015.17.1.54>
- Crank J (1979) *The mathematics of diffusion*. Oxford University Press, Ely House, London
- Davis KL, Martin E, Turko IV, Murad F (2001) Neno
- Dawson VL, Dawson TM, Dawson VL, Dawson TM et al (1991) Nitric oxide mediates glutamate neurotoxicity in primary. *Proc Natl Acad Sci USA* 88:6368–6371
- Dormanns K, Brown RG, David T (2016) The role of nitric oxide in neurovascular coupling. *J Theor Biol* 394:1–17. <https://doi.org/10.1016/j.jtbi.2016.01.009>
- Dupont G, Erneux C (1997) Simulations of the effects of inositol and activities on  $Ca^{2+}$  + oscillations. 22:321–331
- Dupont G, Swillens S, Clair C et al (2000) Hierarchical organization of calcium signals in hepatocytes: from experiments to models. *Biochim Biophys Acta - Mol Cell Res* 1498:134–152. [https://doi.org/10.1016/S0167-4889\(00\)00090-2](https://doi.org/10.1016/S0167-4889(00)00090-2)
- Egelman DM, Montague PR (1999) Calcium dynamics in the extracellular space of mammalian neural tissue. *Biophys J* 76:1856–1867. [https://doi.org/10.1016/S0006-3495\(99\)77345-5](https://doi.org/10.1016/S0006-3495(99)77345-5)
- Eskandari Z, Shahraki HE, Naik PA (2021) Flip and generalized flip bifurcations of a two-dimensional discrete-time chemical model. *Math Model Numer Simul Appl* 1:95–101. <https://doi.org/10.53391/mmnsa.2021.01.009>
- Falcke M (2003) Buffers and oscillations in intracellular  $Ca^{2+}$  dynamics. *Biophys J* 84:28–41. [https://doi.org/10.1016/S0006-3495\(03\)74830-9](https://doi.org/10.1016/S0006-3495(03)74830-9)
- Falcke M, Huerta R, Rabinovich MI et al (2000) Modeling observed chaotic oscillations in bursting neurons: the role of calcium dynamics and IP3. *Biol Cybern* 82:517–527. <https://doi.org/10.1007/s004220050604>
- Fogelson AL, Zucker RS (1985) Presynaptic calcium diffusion from various arrays of single channels. Implications for transmitter release and synaptic facilitation. *Biophys J* 48:1003–1017. [https://doi.org/10.1016/S0006-3495\(85\)83863-7](https://doi.org/10.1016/S0006-3495(85)83863-7)
- Garthwaite J (1991) Glutamate, nitric oxide and cell-cell signalling in the nervous system. *Trends Neurosci* 14:60–67. [https://doi.org/10.1016/0166-2236\(91\)90022-M](https://doi.org/10.1016/0166-2236(91)90022-M)
- Garthwaite G, Garthwaite J (1988) Cyclic GMP and cell death in rat cerebellar slices. *Neuroscience* 26:321–326. [https://doi.org/10.1016/0306-4522\(88\)90148-0](https://doi.org/10.1016/0306-4522(88)90148-0)
- Garthwaite J, Garthwaite G, Palmer RMJ, Moncada S (1989) NMDA receptor activation induces nitric oxide synthesis from arginine in rat brain slices. *Eur J Pharmacol Mol Pharmacol* 172:413–416. [https://doi.org/10.1016/0922-4106\(89\)90023-0](https://doi.org/10.1016/0922-4106(89)90023-0)
- Gibson WG, Farnell L, Bennett MR (2007) A computational model relating changes in cerebral blood volume to synaptic activity in neurons. *Neurocomputing* 70:1674–1679. <https://doi.org/10.1016/j.neucom.2006.10.071>
- Huang PL (2004) Nitric oxide and cerebral ischemic preconditioning. *Cell Calcium* 36:323–329. <https://doi.org/10.1016/j.ceca.2004.02.007>
- Iino M (2006)  $Ca^{2+}$ -dependent inositol 1,4,5-trisphosphate and nitric oxide signaling in cerebellar neurons. *J Pharmacol Sci* 100:538–544. <https://doi.org/10.1254/jphs.CPJ06006X>
- Jagtap YD, Adlakha N (2018) Simulation of buffered advection diffusion of calcium in a hepatocyte cell. *Math Biol Bioinforma* 13:609–619. <https://doi.org/10.17537/2018.13.609>
- Jagtap Y, Adlakha N (2019) Numerical study of one-dimensional buffered advection–diffusion of calcium and IP3 in a hepatocyte cell. *Netw Model Anal Heal Inform Bioinforma* 8:1–9. <https://doi.org/10.1007/s13721-019-0205-5>
- Jha A, Adlakha N (2014) Analytical solution of two dimensional unsteady state problem of calcium diffusion in a neuron cell. *J Med Imaging Heal Inform* 4:547–553. <https://doi.org/10.1166/jmih.2014.1282>
- Jha BK, Adlakha N, Mehta MN (2013) Two-dimensional finite element model to study calcium distribution in astrocytes in presence of VGCC and excess buffer. *Int J Model Simul Comput*. <https://doi.org/10.1142/S1793962312500304>
- Jha BK, Adlakha N, Mehta MN (2014) Two-dimensional finite element model to study calcium distribution in astrocytes in presence of excess buffer. *Int J Biomath* 7:1–11. <https://doi.org/10.1142/S1793524514500314>
- Kaul M, Garden GA, Lipton SA (2001) Pathways to neuronal injury and apoptosis in HIV-associated dementia. *Nature* 410:988–994. <https://doi.org/10.1038/35073667>
- Kavdia M, Tsoukias NM, Popel AS (2002) Model of nitric oxide diffusion in an arteriole: impact of hemoglobin-based blood substitutes. *Am J Physiol - Hear Circ Physiol* 282:2245–2253. <https://doi.org/10.1152/ajpheart.00972.2001>
- Kiss JP, Vizi ES (2001) Nitric oxide: a novel link between synaptic and nonsynaptic transmission. *Trends Neurosci* 24:211–215. [https://doi.org/10.1016/S0166-2236\(00\)01745-8](https://doi.org/10.1016/S0166-2236(00)01745-8)
- Kohlmeier KA, Leonard CS (2006) Transmitter modulation of spike-evoked calcium transients in arousal related neurons: Muscarinic inhibition of SNX-482-sensitive calcium influx. *Eur J Neurosci* 23:1151–1162. <https://doi.org/10.1111/j.1460-9568.2006.04640.x>
- Kotwani M, Adlakha N, Mehta MN (2012) Numerical model to study calcium diffusion in fibroblasts cell for one dimensional unsteady state case. *Appl Math Sci* 6:5063–5072
- Kotwani M, Adlakha N, Mehta MN (2014) Finite element model to study the effect of buffers, source amplitude and source geometry on spatiooral calcium distribution in fibroblast cell. *J Med Imaging Heal Inform* 4:840–847. <https://doi.org/10.1166/jmih.2014.1328>
- Kourosh-Arabi M, Hosseini N, Mohsenzadegan M et al (2020) Neurophysiologic implications of neuronal nitric oxide synthase. *Rev Neurosci* 31:617–636. <https://doi.org/10.1515/revneuro-2019-0111>
- Lipton SA, Choi YB, Pan ZH et al (1993) A redox-based mechanism for the neuroprotective and neurodestructive effects of nitric oxide and related nitroso-compounds. *Nature* 364:626–632. <https://doi.org/10.1038/364626a0>
- Li YX, Rinzel J (1994) Equations for InsP3 receptor-mediated  $[Ca^{2+}]_i$  oscillations derived from a detailed kinetic model: a Hodgkin-Huxley like formalism. *J Theor Biol* 166:461–473
- Llinas R (1979) The role of calcium in neuronal function. *Neurosci Fourth Study Progr*, p 555–571
- López-Jaramillo P (2000) Calcium, nitric oxide, and preeclampsia. *Semin Perinatol* 24:33–36. [https://doi.org/10.1016/S0146-0005\(00\)80052-X](https://doi.org/10.1016/S0146-0005(00)80052-X)

- Lo EH, Dalkara T, Moskowitz MA (2003) Neurological diseases: mechanisms, challenges and opportunities in stroke. *Nat Rev Neurosci* 4:399–414. <https://doi.org/10.1038/nrn1106>
- Manhas N, Pardasani KR (2014) Mathematical model to study IP3 dynamics dependent calcium oscillations in pancreatic acinar cells. *J Med Imaging Heal Inform* 4:874–880. <https://doi.org/10.1166/jmihi.2014.1333>
- Manhas N, Sneyd J, Pardasani KR (2014) Modelling the transition from simple to complex  $\text{Ca}^{2+}$  oscillations in pancreatic acinar cells. *J Biosci* 39:463–484. <https://doi.org/10.1007/s12038-014-9430-3>
- Miyazaki S (1993) IP3 Receptor-mediated spatial and temporal  $\text{Ca}^{2+}$  signaling of the cell, 409–434
- Moro MA, Cárdenas A, Hurtado O, et al (2004) Role of nitric oxide after brain ischaemia. 36:265–275. <https://doi.org/10.1016/j.ceca.2004.02.011>
- Naik PA, Pardasani KR (2013) Finite element model to study effect of  $\text{Na}^+/\text{K}^+$  pump and  $\text{Na}^+/\text{Ca}^{2+}$  exchanger on calcium distribution in oocytes in presence of buffers. *Asian J Math Stat* 7:21–28. <https://doi.org/10.3923/ajms.2014.21.28>
- Naik PA, Pardasani KR (2015a) One dimensional finite element model to study calcium distribution in oocytes in presence of VGCC, RyR and buffers. *J Med Imaging Heal Inform* 5:471–476. <https://doi.org/10.1166/jmihi.2015.1431>
- Naik PA, Pardasani KR (2015b) Two dimensional finite element model to study calcium distribution in oocytes. *J Multiscale Model* 06:1450002. <https://doi.org/10.1142/s1756973714500024>
- Naik PA, Pardasani KR (2016) Finite element model to study calcium distribution in oocytes involving voltage gated  $\text{Ca}^{2+}$  channel, ryanodine receptor and buffers. *Alexandria J Med* 52:43–49. <https://doi.org/10.1016/j.ajme.2015.02.002>
- Naik PA, Pardasani KR (2019) Three-dimensional finite element model to study effect of RyR calcium channel, ER leak and SERCA pump on calcium distribution in oocyte cell. *Int J Comput Methods* 16:1–19. <https://doi.org/10.1142/S0219876218500913>
- Naik PA, Zu J (2020) Modeling and simulation of spatial-temporal calcium distribution in T lymphocyte cell by using a reaction-diffusion equation. *J Bioinform Comput Biol*. <https://doi.org/10.1142/S0219720020500134>
- Öziş T, Aksan EN, Özdeş A (2003) A finite element approach for solution of Burgers' equation. *Appl Math Comput* 139:417–428. [https://doi.org/10.1016/S0096-3003\(02\)00204-7](https://doi.org/10.1016/S0096-3003(02)00204-7)
- Panday S, Pardasani KR (2013) Finite element model to study effect of advection diffusion and  $\text{Na}^+/\text{Ca}^{2+}$  exchanger on  $\text{Ca}^{2+}$  distribution in oocytes. *J Med Imaging Heal Inform* 3:374–379. <https://doi.org/10.1166/jmihi.2013.1184>
- Pathak KB, Adlakha N (2015) Finite element model to study calcium signalling in cardiac myocytes involving pump, leak and excess buffer. *J Med Imaging Heal Inform* 5:683–688. <https://doi.org/10.1166/jmihi.2015.1443>
- Pathak K, Adlakha N (2016) Finite element model to study two dimensional unsteady state calcium distribution in cardiac myocytes. *Alexandria J Med* 52:261–268. <https://doi.org/10.1016/j.ajme.2015.09.007>
- Pawar A, Pardasani KR (2022a) Simulation of disturbances in interdependent calcium and  $\beta$ -amyloid dynamics in the nerve cell. *Eur Phys J plus* 1378(137):1–23. <https://doi.org/10.1140/EPJP/S13360-022-03164-X>
- Pawar A, Pardasani KR (2022b) Effect of disturbances in neuronal calcium and IP3 dynamics on  $\beta$ -amyloid production and degradation. *Cogn Neurodynamics* 2022:1–18. <https://doi.org/10.1007/S11571-022-09815-0>
- Pawar A, Raj Pardasani K (2022c) Effects of disorders in interdependent calcium and IP3 dynamics on nitric oxide production in a neuron cell. *Eur Phys J plus* 137:543. <https://doi.org/10.1140/EPJP/S13360-022-02743-2>
- Peunova N, Enikolopov G (1993) Amplification of calcium-induced gene transcription by nitric oxide in neuronal cells. *Nature* 364:450–453. <https://doi.org/10.1038/364450a0>
- Plank MJ, Wall DJN, David T (2007) The role of endothelial calcium and nitric oxide in the localisation of atherosclerosis. *Math Biosci* 207:26–39. <https://doi.org/10.1016/j.mbs.2006.08.017>
- Prast H, Philippu A (2001) Nitric oxide as modulator of neuronal function. *Prog Neurobiol* 64:51–68. [https://doi.org/10.1016/S0301-0082\(00\)00044-7](https://doi.org/10.1016/S0301-0082(00)00044-7)
- Salter M, Knowles G (1991) Activity of  $\text{Ca}^{2+}$ -dependent and  $\text{Ca}^{2+}$ -independent nitric oxide S. *FEBS Lett* 291:145–149
- Singh N, Adlakha N (2019a) Nonlinear dynamic modeling of 2-dimensional interdependent calcium and inositol 1,4,5-trisphosphate in cardiac myocyte. *Math Biol Bioinforma* 14:290–305. <https://doi.org/10.17537/2019.14.290>
- Singh N, Adlakha N (2019b) A mathematical model for interdependent calcium and inositol 1,4,5-trisphosphate in cardiac myocyte. *Netw Model Anal Heal Inform Bioinforma*. <https://doi.org/10.1007/s13721-019-0198-0>
- Singh N, Adlakha N (2020) Effect of source geometry on interdependent calcium and inositol 1; 4; 5-trisphosphate dynamics in a cardiac myocyte cell. *Springer Proc Math Stat* 308:75–83. [https://doi.org/10.1007/978-981-15-1338-1\\_6](https://doi.org/10.1007/978-981-15-1338-1_6)
- Smith GD (1996) Analytical steady-state solution to the rapid buffering approximation near an open  $\text{Ca}^{2+}$  channel. *Biophys J* 71:3064–3072. [https://doi.org/10.1016/S0006-3495\(96\)79500-0](https://doi.org/10.1016/S0006-3495(96)79500-0)
- Smith GD, Wagner J, Keizer J (1996) Validity of the rapid buffering approximation near a point source of calcium ions. *Biophys J* 70:2527–2539. [https://doi.org/10.1016/S0006-3495\(96\)79824-7](https://doi.org/10.1016/S0006-3495(96)79824-7)
- Sneyd J, Tsaneva-Atanasova K, Bruce JIE et al (2003) A model of calcium waves in pancreatic and parotid acinar cells. *Biophys J* 85:1392–1405. [https://doi.org/10.1016/S0006-3495\(03\)74572-X](https://doi.org/10.1016/S0006-3495(03)74572-X)
- Stamler JS, Meissner G (2001) Physiology of nitric oxide in skeletal muscle. *Physiol Rev* 81:209–237. <https://doi.org/10.1152/physrev.2001.81.1.209>
- Tewari S, Pardasani KR (2008) Finite difference model to study the effects of  $\text{Na}^+$  influx on cytosolic  $\text{Ca}^{2+}$  diffusion. *World Acad Sci Eng Technol* 670–675
- Tewari SG, Pardasani KR (2010) Finite element model to study two dimensional unsteady state cytosolic calcium diffusion in presence of excess buffers. *IAENG Int J Appl Math* 40:1–5
- Tewari V, Tewari S, Pardasani KR (2011) A model to study the effect of excess buffers and  $\text{Na}^+$  ions on  $\text{Ca}^{2+}$  diffusion in neuron cell. *World Acad Sci Eng Technol* 76:41–46. <https://doi.org/10.5281/zenodo.1054988>
- Tewari SG, Pardasani KR (2012) Modeling effect of sodium pump on calcium oscillations in neuron cells. *J Multiscale Model* 04:1250010. <https://doi.org/10.1142/s1756973712500102>
- Thomsen L, neurology JO-C opinion in, 2001 undefined Nitric oxide in primary headaches. *journals.lww.com*
- Tong XY, Ying J, Pimentel DR et al (2008) High glucose oxidizes SERCA cysteine-674 and prevents inhibition by nitric oxide of smooth muscle cell migration. *J Mol Cell Cardiol* 44:361–369. <https://doi.org/10.1016/j.yjmcc.2007.10.022>
- Torreilles F, Salman-Tabcheh S, Guérin MC, Torreilles J (1999) Neurodegenerative disorders: the role of peroxynitrite. *Brain Res Rev* 30:153–163. [https://doi.org/10.1016/S0165-0173\(99\)00014-4](https://doi.org/10.1016/S0165-0173(99)00014-4)
- Tripathi A, Adlakha N (2011) Closed form solution to problem of calcium diffusion in cylindrical shaped neuron cell. *World Acad Sci Eng Technol* 80:739–742
- Tsoukias NM (2008) Nitric oxide bioavailability in the microcirculation: insights from mathematical models. *Microcirculation* 15:813–834. <https://doi.org/10.1080/10739680802010070>

- Van Liew H, Raychaudhuri S (1997) Modeling in physiology. *J Appl Physiol* 82:2045–2053
- Verkhatsky A (2002) The endoplasmic reticulum and neuronal calcium signalling. *Cell Calcium* 32:393–404. <https://doi.org/10.1016/S0143416002001896>
- Vincent SR (1994) Nitric oxide: a radical neurotransmitter in the central nervous system. *Prog Neurobiol* 42:129–160. [https://doi.org/10.1016/0301-0082\(94\)90023-X](https://doi.org/10.1016/0301-0082(94)90023-X)
- Vincent SR (2010) Nitric oxide neurons and neurotransmission. *Prog Neurobiol* 90:246–255. <https://doi.org/10.1016/j.pneurobio.2009.10.007>
- Wagner J, Keizer J (1994) Effects of rapid buffers on  $\text{Ca}^{2+}$  diffusion and  $\text{Ca}^{2+}$  oscillations. *Biophys J* 67:447–456. [https://doi.org/10.1016/S0006-3495\(94\)80500-4](https://doi.org/10.1016/S0006-3495(94)80500-4)
- Wagner J, Fall CF, Hong F et al (2004) A wave of IP3 production accompanies the fertilization  $\text{Ca}^{2+}$  wave in the egg of the frog, *Xenopus laevis*: theoretical and experimental support. *Cell Calcium* 35:433–447. <https://doi.org/10.1016/j.ceca.2003.10.009>
- Weiner CP, Lizasoain I, Baylis SA et al (1994) Induction of calcium-dependent nitric oxide synthases by sex hormones. *Proc Natl Acad Sci USA* 91:5212–5216. <https://doi.org/10.1073/pnas.91.11.5212>
- Wojda U, Salinska E, Kuznicki J (2008) Calcium ions in neuronal degeneration. *IUBMB Life* 60:575–590. <https://doi.org/10.1002/iub.91>
- Wood J, Garthwaite J (1994) Models of the diffusional spread of nitric oxide: implications for neural nitric oxide signalling and its pharmacological properties. *Neuropharmacology* 33:1235–1244. [https://doi.org/10.1016/0028-3908\(94\)90022-1](https://doi.org/10.1016/0028-3908(94)90022-1)
- Wood PL, Emmett MR, Rao TS et al (1990) Inhibition of nitric oxide synthase blocks N-methyl-D-aspartate-, quisqualate-, kainate-, harmaline-, and pentylentetrazole-dependent increases in cerebellar cyclic GMP in vivo. *J Neurochem* 55:346–348. <https://doi.org/10.1111/j.1471-4159.1990.tb08859.x>
- Young GWDE, Keizer J (1992) A single-pool inositol 1,4,5-trisphosphate-receptor-based model for agonist-stimulated oscillations in  $\text{Ca}^{2+}$  concentration. *Biophysics (Oxf)* 89:9895–9899
- Zhang L, Dawson VL, Dawson TM (2006) Role of nitric oxide in Parkinson's disease. *Pharmacol Ther* 109:33–41. <https://doi.org/10.1016/j.pharmthera.2005.05.007>

**Publisher's Note** Springer Nature remains neutral with regard to jurisdictional claims in published maps and institutional affiliations.

Springer Nature or its licensor (e.g. a society or other partner) holds exclusive rights to this article under a publishing agreement with the author(s) or other rightsholder(s); author self-archiving of the accepted manuscript version of this article is solely governed by the terms of such publishing agreement and applicable law.